

Universal Graph Backdoor Defense: A Feature-based Homophily Perspective

Mengting Pan

mengting.pan@unsw.edu.au
The University of New South Wales
Sydney, Australia

Chen Chen

chenc@uow.edu.au
University of Wollongong
Wollongong, Australia

Fan Li

fan.li8@unsw.edu.au
The University of New South Wales
Sydney, Australia

Xiaoyang Wang

xiaoyang.wang1@unsw.edu.au
The University of New South Wales
Sydney, Australia

Abstract

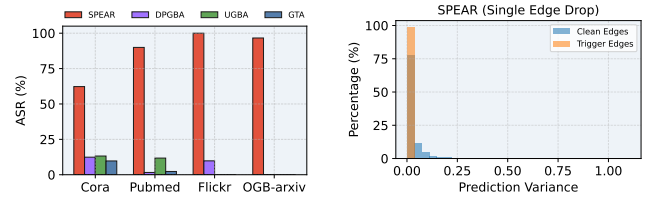
Graph neural networks (GNNs) have achieved remarkable success in relational learning. However, their vulnerability to graph backdoor attacks (GBAs) poses a significant barrier to broader adoption in high-stakes applications. Despite recent advances in graph backdoor defense (GBD), existing methods primarily focus on subgraph-based GBAs, relying on the assumption that poisoned target nodes are explicitly connected to subgraph triggers. Our empirical results reveal that such structure-centric approaches fail to defend against emerging feature-based GBAs that preserve graph topology. Therefore, in this paper, we study a novel problem of universal graph backdoor defense. First, we investigate the shared effects of both attack types from a feature-based homophily perspective, which characterizes local feature consistency between nodes and their neighborhoods. Thorough theoretical and empirical analyses demonstrate that, regardless of trigger mechanisms, backdoors induced by GBAs exhibit lower feature-based homophily than clean nodes, indicating a discrepancy in local feature similarity. Motivated by this insight, we propose to leverage node-level local feature consistency, modeled by a neighbor-aware reconstruction loss, to distinguish backdoors from clean nodes. Then, a robust training strategy is developed to eliminate trigger effects while reducing noise induced by detection uncertainty. Extensive experiments demonstrate that our framework significantly degrades the attack success rate and maintains competitive clean accuracy under both subgraph-based and feature-based attacks.

Keywords

Safety, Robustness, Backdoor attack, Graph neural network

1 Introduction

Graph-structured data [1, 27, 38] is widely used for relational modeling across many real-world domains, including social networks [8, 13], molecular biology [2, 22], and financial systems [15, 40]. To effectively learn from such data, Graph Neural Networks (GNNs) [14, 19, 28] have emerged as a prevalent and powerful model, leveraging message passing to encode local structural patterns and node features. Despite their remarkable success, recent studies [5, 7, 35] reveal that GNNs are vulnerable to backdoor attacks. In these attacks, adversaries inject malicious triggers into selected target nodes and manipulate their labels toward a predefined target class, causing the



(a) The performance of RIGBD. (b) SPEAR (Single Edge Drop).

Figure 1: (a): Attack success rate (%) of different graph backdoor attacks under RIGBD. (b): Prediction variance caused by dropping trigger edges and clean edges.

trained model to learn the spurious trigger-class association and produce targeted misclassification during inference. This vulnerability hinders the safe deployment of GNNs in high-stakes scenarios such as banking systems, cybersecurity, and healthcare.

Existing graph backdoor attacks primarily focus on designing subgraph-based triggers to manipulate local neighborhood patterns around poisoned nodes. For example, SBA [34] adopts random or sampled subgraphs as triggers, while GTA [29] introduces learnable triggers that adapt to individual targets. To further enhance stealthiness, UGBA [5] and DPGBA [35] incorporate regularization mechanisms to generate similarity-preserving and in-distribution triggers, respectively, making trigger nodes less distinguishable from clean ones. To defend against the above subgraph-based attacks, several initial methods, such as Prune [5] and OD [35], have been proposed. However, these approaches are tailored to specific backdoor patterns and thus remain effective only for particular attack methods. To address this limitation, RIGBD [36] proposes to identify poisoned target nodes through prediction variance under random edge perturbations and further introduces a robust training strategy to eliminate their adverse effects. This enables a more effective and generalizable defense against subgraph-based attacks.

Despite achieving state-of-the-art performance against backdoor attacks based on subgraph triggers, RIGBD fails on SPEAR [7], a recent feature-based attack that implants triggers into node attributes without altering graph topology, as shown in Fig. 1(a). Specifically, we observe that although RIGBD consistently reduces the attack success rate (ASR) of subgraph-based attacks to below 15% across datasets, SPEAR still achieves over 60% ASR under RIGBD’s defense, even exceeding 89% on most datasets. This failure arises because

RIGBD relies on the empirical assumption that removing edges associated with backdoor triggers induces a large prediction variance on poisoned target nodes. In contrast, feature-based attacks do not introduce explicit structural triggers, which invalidates this assumption. To substantiate this claim, we iteratively drop the neighboring edges around each node and measure the resulting variance in predictions. Our empirical results in Fig. 1(b) show that under SPEAR, edge dropping around poisoned nodes induces prediction variance indistinguishable from that of clean nodes, further explaining the ineffectiveness of RIGBD against feature-based attacks.

To bridge this research gap, we first investigate the shared effects in subgraph-based and feature-based backdoor attacks. Intuitively, regardless of whether triggers are attached to poisoned targets in the form of subgraphs or directly injected into node attributes, the feature similarity between poisoned targets (or trigger nodes) and their surrounding neighbors may be perturbed. Motivated by this, we introduce a novel concept termed *feature-based homophily*, which characterizes the feature consistency between each node and its local neighborhood. Through rigorous theoretical analysis in Sec. 4.1, we show that, compared with clean nodes, poisoned targets exhibit lower feature-based homophily with respect to their surrounding neighbors, indicating stronger feature inconsistency within local neighborhoods. Empirical results in Sec. 4.2 across multiple datasets further strengthen this theoretical finding. This homophily discrepancy unifies the intrinsic effects of both attack types and naturally provides an effective discriminative signal for identifying backdoors, including both triggers and poisoned targets.

Based on these insights, we propose CoGBD (**C**onsistency-guided **G**raph **B**ackdoor **D**efense), a novel graph backdoor defense framework that leverages the deviation of feature consistency within local neighborhoods. To the best of our knowledge, CoGBD is the first universal graph backdoor defense capable of effectively defending against both subgraph-based and feature-based attacks. Overall, CoGBD adopts a two-stage pipeline. Motivated by the above analysis, in the first stage, we design tri-directional reconstruction objectives to model feature consistency within the local neighborhood of each individual node, where nodes exhibiting large reconstruction errors are identified as potential backdoors. In the second stage, we develop a noise-aware robust training strategy that minimizes overconfident predictions for candidate poisoned nodes using adaptive weights inversely related to their reconstruction errors. This design effectively counteracts the impacts of triggers while mitigating noise introduced by potentially imprecise backdoor detection. Our main contributions are summarized as follows:

- We empirically show the ineffectiveness of state-of-the-art graph backdoor defenses against feature-based attacks and study a novel problem of universal graph backdoor defense.
- We unify the effects of both subgraph-based and feature-based graph backdoor attacks from a feature-based homophily perspective. Our theoretical and empirical analyses uncover a local feature consistency gap that provides practical guidance for identifying backdoors.
- We propose CoGBD, the first universal graph backdoor defense framework, consisting (i) a reconstruction-driven

backdoor detection stage that leverages the feature consistency gap and (ii) a noise-aware robust training stage that adaptively counteracts trigger influence.

- Extensive experiments demonstrate the effectiveness of CoGBD in defending against both subgraph-based and feature-based attacks while maintaining clean accuracy.

2 Related Works

Graph Backdoor Attacks. Graph backdoor attacks (GBAs) [16, 26, 30, 31] expose a severe vulnerability of GNNs, where an adversary implants triggers into a small set of training nodes so that the trained model associates the trigger with a target label. At test time, any node carrying the trigger is misclassified to the target class, while predictions on clean nodes remain largely unaffected. Most existing GBAs instantiate triggers as subgraphs by manipulating local connectivity patterns. SBA [34] injects a universal subgraph into selected nodes, and GTA [29] further learns adaptive triggers via a generator. To improve stealthiness, UGBA [5] encourages similarity between trigger nodes and the attached targets. Subsequent studies show that many of these triggers are out-of-distribution and remain distinguishable from clean neighborhoods [35]. DPGBA [35] improves stealthiness by generating in-distribution triggers through adversarial optimization. Beyond structural manipulation, feature-based graph backdoor attacks inject triggers directly into node attributes while keeping the graph topology intact. SPEAR [7] exemplifies this paradigm by embedding attack signals purely in node features, significantly increasing stealthiness and challenging defenses that rely on structural irregularities.

Graph Backdoor Defense. Compared with the rapidly growing studies on graph backdoor attacks, graph backdoor defense (GBD) methods remain limited. Most existing GBD methods are designed for subgraph-based attack and rely on the assumption that backdoor triggers introduce explicit structural irregularities. For example, Prune [5] weakens potential trigger effects by removing edges between node pairs with low feature similarity, while Outlier Detection (OD) [35] identifies trigger nodes that deviate from the distribution of clean data and isolates their connections from the remaining graph. However, these methods are typically tailored to specific trigger structures and are effective only for particular subgraph-based attack patterns. To overcome this limitation, RIGBD [36] focuses on poisoned target nodes by exploiting the model’s sensitivity to random edge dropping and incorporating robust training to eliminate trigger effects, enabling more generalizable defense in various subgraph-based backdoor attacks. While RIGBD achieves strong performance against a wide range of subgraph-based backdoor attacks, it becomes less reliable in recent feature-based GBAs, where backdoor triggers are embedded in node attributes and the graph topology is largely preserved. This gap motivates us to develop a unified defense framework that remains effective against both subgraph-based and feature-based backdoor attacks.

3 Preliminaries

Notations. Let $\mathcal{G} = (\mathcal{V}, \mathcal{E}, \mathbf{X})$ denote an attributed graph, where $\mathcal{V} = \{v_1, \dots, v_N\}$ is the set of N nodes, $\mathcal{E} \subseteq \mathcal{V} \times \mathcal{V}$ is the set of E edges, and $\mathbf{X} \in \mathbb{R}^{N \times F}$ is the node attribute matrix, with each node v_i associated with a feature vector $\mathbf{x}_i \in \mathbb{R}^F$. The one-hop

neighborhood of node v is denoted by $\mathcal{N}(v) = \{u : (u, v) \in \mathcal{E}\}$. $\mathbf{A} \in \mathbb{R}^{N \times N}$ is the adjacency matrix of the graph \mathcal{G} , where $A_{ij} = 1$ if $(v_i, v_j) \in \mathcal{E}$, and $A_{ij} = 0$ otherwise. We denote the normalized adjacency matrix with self-loops as $\tilde{\mathbf{A}} = \mathbf{D}^{-1/2}(\mathbf{A} + \mathbf{I})\mathbf{D}^{-1/2}$, where \mathbf{I} is the identity matrix and \mathbf{D} is the diagonal degree matrix with $D_{ii} = \sum_j (\mathbf{A} + \mathbf{I})_{ij}$. In this paper, we focus on the semi-supervised node classification task in the inductive setting. During training, we are given a graph $\mathcal{G}_T = (\mathcal{V}_T, \mathcal{E}_T, \mathbf{X}_T)$. We use $\mathcal{V}_C \subseteq \mathcal{V}_T$ and $\mathcal{V}_B \subseteq \mathcal{V}_T$ to denote the clean and backdoored node sets, respectively. Nodes in \mathcal{V}_C are labeled with clean labels, whereas nodes in \mathcal{V}_B are labeled with the target label y_t . The remaining nodes $\mathcal{V}_T \setminus (\mathcal{V}_C \cup \mathcal{V}_B)$ are unlabeled. At inference time, we are given an unseen graph $\mathcal{G}_U = (\mathcal{V}_U, \mathcal{E}_U, \mathbf{X}_U)$. The node set \mathcal{V}_U consists of clean and backdoored test nodes, denoted by \mathcal{V}_{UC} and \mathcal{V}_{UB} , respectively. Notably, \mathcal{G}_U is disjoint from the training graph, i.e., $\mathcal{V}_U \cap \mathcal{V}_T = \emptyset$.

Graph Neural Networks (GNNs). Most existing GNNs adopt a message-passing paradigm, in which each node $v \in \mathcal{V}$ is associated with a representation vector h_v that is iteratively updated over K layers. At each layer, node representations are first aggregated from local neighborhoods $\mathcal{N}(v)$ and then transformed by a learnable encoder. Formally, for common GNN models such as GCN [12] and GAT [24], the representation of node v at the k -th layer is updated as: $h_v^{(k)} = \text{ENC}\left(\text{AGGR}\left(\{h_u^{(k-1)} : u \in \mathcal{N}(v) \cup \{v\}\}\right)\right)$, where $\text{AGGR}(\cdot)$ denotes a permutation-invariant neighborhood aggregation operator and $\text{ENC}(\cdot)$ is a learnable transformation.

Threat Model. We consider the common gray-box backdoor attack [5, 7, 29, 35, 36], where the attacker has access to the training graph \mathcal{G}_T , but has no knowledge of the victim GNN architecture or parameters. The attacker aims to attach backdoor triggers, i.e., nodes, subgraphs, or feature perturbations, into a small set of nodes \mathcal{V}_B and assign them the target label y_t , resulting in a backdoored graph $\mathcal{G}_B = (\mathcal{V}'_T, \mathcal{E}'_T, \mathbf{X}'_T)$. A GNN model trained on \mathcal{G}_B is expected to behave normally on clean nodes while being misguided by the backdoor trigger to classify nodes attached with triggers as y_t . Formally, given a surrogate GNN model f_s , which the attacker uses as a proxy to design and optimize backdoor triggers, the attack objective can be expressed as: $\min_{f_s} \sum_{v \in \mathcal{V}_B} \ell(f_s(v), y_t) + \sum_{u \in \mathcal{V}_C} \ell(f_s(u), y_u)$, where $\ell(\cdot, \cdot)$ denotes the classification loss.

Defender's Knowledge and Objective. Unlike prior graph backdoor defenses [5, 35, 36] that are tailored to subgraph-based attacks and do not generalize to feature-based triggers, we study a universal, attack-agnostic defense setting. The defender only has access to the backdoored training graph \mathcal{G}_B , without prior knowledge of the attack type, the poisoned node set \mathcal{V}_B , or the target label y_t . Given a backdoored graph \mathcal{G}_B , our objective is to train a GNN model f_g that can defend against backdoor triggers during inference while preserving accuracy on clean data, which is formally defined as: $\min_{f_g} \sum_{v \in \mathcal{V}_{UC}} \ell(f_g(v), y_v) - \sum_{u \in \mathcal{V}_{UB}} \ell(f_g(u), y_t)$, where $\ell(\cdot, \cdot)$ denotes the classification loss.

4 A Unified View of Graph Backdoor Attacks

In this section, we provide a unified view of graph backdoor attacks. By rethinking both subgraph-based and feature-based GBAs from a novel feature-based homophily perspective, we theoretically and empirically show that seemingly different attack strategies induce

common intrinsic effects at the representation level. This unified perspective decouples the analysis from specific trigger designs, exposes the fundamental mechanisms shared across GBAs, and facilitates the design of the universal backdoor defense strategy.

4.1 Theoretical Analysis

Feature-based Homophily. We posit that both subgraph-based and feature-based GBAs, despite employing different trigger forms, can implicitly alter the consistency between a node and its local neighborhood. Specifically, subgraph triggers and malicious feature perturbations may disrupt the alignment between node attributes and surrounding structures, even when the overall graph topology is preserved. To characterize this consistency, we introduce a novel *feature-based homophily* metric:

DEFINITION 1 (FEATURE-BASED HOMOPHILY). *The feature-based homophily of a node v is defined as the similarity between its features and the aggregated features of its neighboring nodes:*

$$\mathcal{H}_{\text{feat}}(v) = \text{sim}(x_v, \text{AGGR}\{x_u : u \in \mathcal{N}(v)\}), \quad (1)$$

where $\text{sim}(\cdot, \cdot)$ denotes the similarity metric (e.g., cosine similarity).

How Effective GBAs Affect Message Passing in GNNs. We begin by analyzing how graph backdoor attacks (GBAs) affect message passing and the resulting node representations in GNNs. To this end, consider a general backdoored graph $\mathcal{G}_B = (\mathbf{A} + \Delta\mathbf{A}, \mathbf{X} + \Delta\mathbf{X}, \tilde{\mathbf{Y}})$, where $\Delta\mathbf{A}$ and $\Delta\mathbf{X}$ denote the induced perturbations on structure and features, respectively, and $\tilde{\mathbf{Y}}$ denotes the poisoned label set, with target nodes assigned the target class y_t . Let $\mathbf{H}^{(l)} = \tilde{\mathbf{A}}^l \mathbf{X}$ denote the node representations after l layers of message passing, and let $h_v^{(l)} \triangleq [\mathbf{H}^{(l)}]_v$ be the representation of node v . The following lemma characterizes the shift in hidden representations after message passing under attacks.

LEMMA 1. *Let $h_v^{(l)}$ and $h'_v{}^{(l)}$ denote the l -th layer representations of a target node v on the clean and backdoored graphs \mathcal{G}_T and \mathcal{G}_B , respectively. We further denote $\pi_{vu}^{(l)} \triangleq (\tilde{\mathbf{A}}^l)_{vu}$, $\pi'_{vu}{}^{(l)} \triangleq ((\tilde{\mathbf{A}} + \Delta\tilde{\mathbf{A}})^l)_{vu}$. Then, the representation shift $\Delta h_v^{(l)} \triangleq h'_v{}^{(l)} - h_v^{(l)}$ can be written as:*

$$\Delta h_v^{(l)} = \sum_{u \in \mathcal{V}} (\pi'_{vu}{}^{(l)} - \pi_{vu}^{(l)}) x_u + \sum_{u \in \mathcal{V}} \pi'_{vu}{}^{(l)} \Delta x_u, \quad (2)$$

where x_u is the original feature vector of node u and Δx_u denotes the feature perturbation applied on node u .

PROOF. The proof is provided in Appendix A.1. \square

We next provide the necessary condition under which the above perturbations cause targeted nodes to be misclassified.

LEMMA 2. *Consider a targeted graph backdoor attack on node v with target class y_t . The GNN classifier produces logits $z_{v,c} = \mathbf{w}_c^\top h_v^{(l)}$, where \mathbf{w}_c is the class-specific weight vector. The predicted probability for class c is $p_{v,c} = \frac{\exp(z_{v,c})}{\sum_{c'} \exp(z_{v,c'})}$. Let $\ell_{\text{CE}}(v) = -\log p_{v,y_t}$ be the target-class cross-entropy loss. For a small representation shift $\Delta h_v^{(l)}$ induced by the trigger, a necessary condition for decreasing $\ell_{\text{CE}}(v)$ is:*

$$\left\langle \mathbf{w}_{y_t} - \bar{\mathbf{w}}_v, \Delta h_v^{(l)} \right\rangle > 0, \quad (3)$$

where $\bar{\mathbf{w}}_v \triangleq \sum_c p_{v,c} \mathbf{w}_c$ denotes the expected classifier weight under the current predictive distribution of node v .

Table 1: Feature-based homophily across GBAs.

Attack	Node Types	Cora	Pubmed	Flickr	OGB-arxiv
GTA	Clean Nodes	0.1767	0.2647	0.3201	0.8346
	Target Nodes	0.1332	0.1439	0.2273	0.5847
	Trigger Nodes	-0.1166	-0.0461	-0.1060	-0.1012
UGBA	Clean Nodes	0.1767	0.2647	0.3201	0.8346
	Target Nodes	0.1253	0.1936	0.2646	0.7095
	Trigger Nodes	0.1578	0.2019	0.2774	0.8001
DPGBA	Clean Nodes	0.1767	0.2647	0.3201	0.8346
	Target Nodes	0.1422	0.1777	0.2716	0.5251
	Trigger Nodes	0.0691	0.0039	-0.1033	0.0914
SPEAR	Clean Nodes	0.1763	0.2642	0.3201	0.8143
	Target Nodes	0.1208	0.0887	0.3098	0.0852

PROOF. The proof is provided in Appendix A.2. \square

Remark. Lemma 1 characterizes how different types of backdoor triggers perturb node representations through message passing. Lemma 2 further reveals that such perturbations are not arbitrary: the induced representation shift must be explicitly aligned with the target class direction of the classifier.

Distributional Shift in Feature-Based Homophily. We now investigate how effective GBAs induce distributional discrepancies in feature-based homophily across node types.

THEOREM 1. *Given a backdoored graph \mathcal{G}_B with clean node set \mathcal{V}_C and backdoored node set \mathcal{V}_B . For any effective graph backdoor attack, the expected feature-based homophily of backdoored nodes is lower than that of clean nodes:*

$$\mathbb{E}_{v \sim \mathcal{V}_B} [\mathcal{H}_{\text{feat}}(v)] < \mathbb{E}_{v \sim \mathcal{V}_C} [\mathcal{H}_{\text{feat}}(v)]. \quad (4)$$

PROOF. The complete proof is provided in Appendix A.3. \square

Remark. Theorem 1 reveals a distributional discrepancy in the expected feature-based homophily between clean and poisoned target nodes under effective graph backdoor attacks. This phenomenon arises consistently across both subgraph-based and feature-based attack paradigms, highlighting a shared effect of GBAs. In particular, subgraph-based attacks manipulate propagation paths to amplify target-aligned signals, indirectly inducing feature-neighborhood mismatch, whereas feature-based attacks directly inject target-aligned attributes that disrupt local consistency. Beyond target nodes, trigger nodes constitute another essential source of backdoor behavior. Their local context is typically designed to maximize attack effectiveness rather than to preserve node-neighborhood consistency. As a result, trigger nodes likewise exhibit pronounced neighborhood inconsistency as well. Further discussion on trigger nodes is provided in Appendix A.4.

4.2 Empirical Analysis

To further validate the above theoretical finding, we empirically evaluate feature-based homophily under four representative GBAs spanning both subgraph-based and feature-based attacks. In particular, we report the average feature-based homophily of clean nodes, poisoned target nodes, and trigger nodes on the backdoored graph, computed via cosine similarity. From Table 1, we observe that both poisoned target nodes and trigger nodes consistently

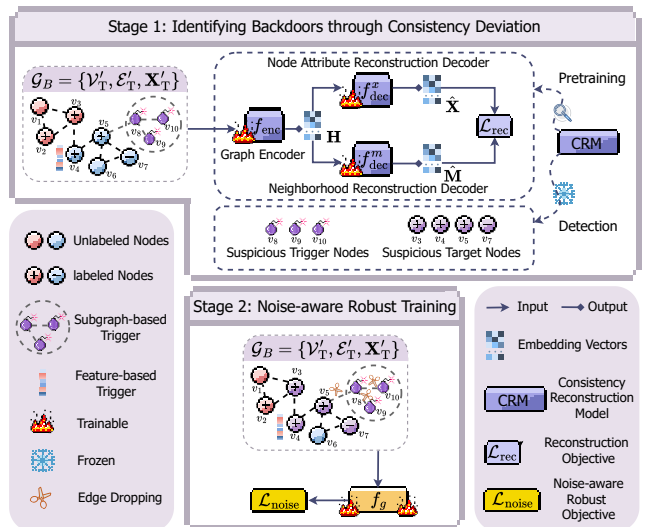


Figure 2: Framework of CoGBD.

exhibit substantially lower feature-based homophily than clean nodes, reflecting a clear homophily discrepancy between backdoors and clean nodes. For poisoned target nodes, this gap is particularly pronounced under feature-based attacks such as SPEAR, where attribute-level triggers directly disrupt local feature-neighborhood alignment (e.g., on OGB-arxiv, target nodes show an approximately 89.5% lower homophily value compared to clean nodes). For trigger nodes, large homophily gaps are observed under subgraph-based attacks such as GTA and DPGBA (e.g., on OGB-arxiv, trigger nodes exhibit about 80% and 90% lower homophily relative to clean nodes, respectively). These results empirically support Theorem 1 and demonstrate that feature-based homophily serves as a stable and discriminative signal for identifying diverse backdoor-induced anomalies across different attack paradigms.

5 Methodology

The above analysis reveals that backdoors exhibit pronounced discrepancies in feature consistency with their surrounding neighborhoods compared to clean nodes. Motivated by this, we propose CoGBD (Consistency-guided Graph Backdoor Defense), a universal graph backdoor defense framework. As depicted in Fig. 2, CoGBD follows a two-stage pipeline. In the first stage, a self-supervised consistency reconstruction model (CRM) is pretrained to capture dominant node-neighborhood patterns and identify both poisoned target nodes and trigger nodes via reconstruction errors. In the second stage, to fully eliminate the influence of malicious nodes while mitigating noise introduced by detection errors, we develop a noise-aware robust training strategy for reliable model defense.

5.1 Identifying Backdoors through Consistency Deviation

Consistency Reconstruction Pretraining. We characterize node-neighborhood consistency via neighborhood-informed reconstruction. Deviations from this consistency hinder reconstruction and lead to larger reconstruction errors, facilitating the identification

of nodes affected by backdoor attacks. To this end, we design a tri-directional reconstruction model that explicitly captures consistency among node attributes, neighborhood context, and their cross-level alignment on the backdoored graph.

Graph Encoder. We use a two-layer GCN with ReLU activations as the graph encoder f_{enc} to map nodes into the latent space. Given a backdoored graph \mathcal{G}_B , the hidden embeddings are computed as:

$$\mathbf{H} = f_{\text{enc}}(\mathbf{X}'_T, \mathbf{A}'_T) \in \mathbb{R}^{N \times d}, \quad (5)$$

where d denotes the hidden dimension, and \mathbf{A}'_T denotes the adjacency matrix of the backdoored graph.

Tri-directional Consistency Reconstruction Objectives. As shown in Sec. 4.1, clean nodes typically dominate a backdoored graph and preserve relatively stable node-neighborhood consistency, in contrast to target and trigger nodes. We therefore learn normal patterns via a tri-directional reconstruction objective, such that backdoored deviations are amplified as larger reconstruction errors. Formally, the overall reconstruction objective \mathcal{L}_{rec} is defined as:

$$\mathcal{L}_{\text{rec}} = \underbrace{\|\mathbf{X}'_T - \hat{\mathbf{X}}\|_F^2}_{\mathcal{L}_{\text{node}}} + \alpha \underbrace{\|\mathbf{M} - \hat{\mathbf{M}}\|_F^2}_{\mathcal{L}_{\text{neigh}}} + \beta \underbrace{\|\mathbf{X}'_T - \hat{\mathbf{M}}\|_F^2}_{\mathcal{L}_{\text{homo}}}, \quad (6)$$

where $\mathbf{M} = \mathbf{A}'_T \mathbf{X}'_T$ denotes the aggregated neighborhood matrix in original graph. Here, $\hat{\mathbf{X}} = f_{\text{dec}}^x(\mathbf{H}) \in \mathbb{R}^{N \times F}$ and $\hat{\mathbf{M}} = f_{\text{dec}}^m(\mathbf{H}) \in \mathbb{R}^{N \times F}$ are the reconstructed node attributes and neighborhood representations, respectively, produced by two lightweight MLP decoders: f_{dec}^x for node-level reconstruction and f_{dec}^m for neighborhood-level reconstruction. The hyperparameters α and β balance the contributions of neighborhood consistency and cross-level alignment.

Terms in Eq. (6) capture complementary aspects of graph consistency: (i) $\mathcal{L}_{\text{node}}$ preserves individual attribute regularity; (ii) $\mathcal{L}_{\text{neigh}}$ models local contextual patterns through neighborhood reconstruction; and (iii) $\mathcal{L}_{\text{homo}}$ enforces cross-level alignment between node attributes and their neighborhoods, corresponding to feature-based homophily. By jointly optimizing these objectives, the reconstruction model is endowed with enhanced expressiveness to capture diverse and fine-grained node-neighborhood consistency patterns. **Detection.** The pretrained consistency reconstruction model is then leveraged to distinguish backdoors from clean nodes. For each node v_i , we define its reconstruction error e_i as:

$$e_i = \|\mathbf{x}_i - \bar{\mathbf{x}}_i\|_2^2 + \alpha \|\mathbf{m}_i - \bar{\mathbf{m}}_i\|_2^2 + \beta \|\mathbf{x}_i - \bar{\mathbf{m}}_i\|_2^2, \quad (7)$$

where $\mathbf{m}_i = [\mathbf{M}]_i$ is the original neighborhood representation of node v_i , and $\bar{\mathbf{x}}_i$ and $\bar{\mathbf{m}}_i$ denote the reconstructed node attribute and neighborhood representation, respectively. Nodes are sorted in descending order of e_i . The top- $\rho\%$ high-risk nodes are considered abnormal, while the remaining nodes are treated as clean.

5.2 Noise-aware Robust Training

The detected backdoors can involve two types of nodes that play distinct roles in graph backdoor attacks. Specifically, they include (i) suspicious trigger nodes, which are typically outside the labeled training set and serve as carriers of backdoor patterns, and (ii) suspicious target nodes, which are labeled with the target class and inject misleading supervision during training.

A simple and effective defense strategy is to remove edges incident to suspicious trigger nodes, which cuts off the most direct

paths through which backdoor signals propagate. However, pruning triggers alone is often insufficient. For in-distribution attacks such as DPGBA, triggers are crafted to mimic target-class neighborhood contexts, making even a model trained on a cleaned graph still responsive to such triggers at test time. Therefore, we further mitigate suspicious target nodes by minimizing the prediction confidence on their observed (typically target-class) labels, encouraging the model to counteract the impact of the trigger. Let \mathcal{V}_L denote the labeled training nodes and \mathcal{V}_S the suspicious target nodes. A natural robust objective for a GNN classifier f_g is therefore:

$$\mathcal{L}_{\text{robust}} = \sum_{v_i \in \mathcal{V}_L} \ell(f_g(v_i), y_i) - \lambda \sum_{v_i \in \mathcal{V}_S} \ell(f_g(v_i), y_i), \quad (8)$$

where $\ell(\cdot, \cdot)$ denotes the cross-entropy loss and λ controls the suppression strength applied to suspicious supervision.

Noise-aware Robust Objective. While Eq. (8) explicitly reduces the influence of suspicious target supervision, its effectiveness still hinges on accurately distinguishing target nodes from clean ones. In practice, graph backdoor attacks are highly sparse and imbalanced: only a small fraction of nodes are poisoned, often accompanied by multiple trigger nodes, while the vast majority remain clean. As a result, hard partitioning inevitably introduces false positives (i.e., clean nodes mistakenly included in \mathcal{V}_S) and false negatives (i.e., poisoned target nodes that remain in \mathcal{V}_L), which may either suppress reliable supervision or leave poisoned signals insufficiently mitigated. To address this issue, we incorporate reconstruction errors as a soft reliability indicator to guide a noise-aware robust training. Formally, we define a suspiciousness score as:

$$s_i = \sigma\left(-\frac{e_i - \mu_e}{\tau \sigma_e}\right), \quad (9)$$

where μ_e and σ_e denote the mean and standard deviation of reconstruction errors over the graph, τ is a temperature parameter and $\sigma(\cdot)$ is the sigmoid function. Intuitively, larger s_i values indicate stronger deviation from normal node-neighborhood consistency. For false positives, moderate s_i should not lead to aggressive suppression, so that reliable supervision is preserved. For false negatives, larger s_i should reduce their effective influence, limiting the impact of poisoned labels even when hard separation fails. Accordingly, we design two noise-aware node weights based on s_i :

$$w_i^L = (1 - s_i)^a, \quad w_i^S = s_i^b, \quad (10)$$

where w_i^L and w_i^S reweight supervision on clean nodes and suspicious nodes, respectively. The exponents a and b are fixed and used to adjust the sharpness of the weights. Therefore, the final noise-aware robust objective is augmented as:

$$\mathcal{L}_{\text{noise}} = \sum_{v_i \in \mathcal{V}_L} w_i^L \ell(f_g(v_i), y_i) - \lambda \sum_{v_i \in \mathcal{V}_S} w_i^S \ell(f_g(v_i), y_i). \quad (11)$$

The training algorithm and the corresponding complexity analysis are provided in Appendix B.

6 Experiments

In this section, we conduct extensive experiments to answer the following research questions:

- **RQ1:** How effective is CoGBD in defending against both subgraph- and feature-based graph backdoor attacks?

Table 2: Statistics of datasets.

Dataset	$ \mathcal{V} $	$ \mathcal{E} $	# Features	# Classes
Cora	2,708	5,429	1,443	7
Pubmed	19,717	44,338	500	3
Flickr	89,250	899,756	500	7
OGB-arxiv	169,343	1,166,243	128	40

- **RQ2:** How well does CoGBD detect backdoors, including trigger nodes and poisoned target nodes?
- **RQ3:** How do the key components contribute to the defense performance of CoGBD?
- **RQ4:** How do different hyperparameters affect the ASR-ACC trade-off of CoGBD?

6.1 Experimental Setup

Datasets. We conduct experiments on four public real-world datasets, i.e., Cora, Pubmed [23], Flickr [32], and OGB-arxiv [11], which are widely used for inductive semi-supervised node classification. Detailed statistics of the datasets are summarized in Table 2.

Attack Methods. To validate the defense capability of CoGBD, we evaluate it against four state-of-the-art graph backdoor attacks, including three subgraph-based attacks (GTA [29], UGBA [5], and DPGBA [35]) and one recent feature-based attack (SPEAR [7]). Detailed descriptions are provided in Appendix C.1.

Competitive Methods. We compare CoGBD with three competitive defense methods tailored for graph backdoor attacks, including Prune [5], OD [35], and RIGBD [36]. In addition, ABL [18], a popular backdoor defense in the image domain, is also included for comparison. Moreover, we incorporate three representative robust GNN models (RobustGCN [39], GNNGuard [33], and randomized smoothing (RS) [25]) to examine whether general robustness architectures can effectively mitigate graph backdoor attacks. Detailed descriptions of these defense methods are provided in Appendix C.2.

Evaluation Protocol. We follow the inductive node classification setting commonly adopted in recent graph backdoor studies [5, 7, 35, 36]. Specifically, each dataset is randomly split into two disjoint subgraphs, denoted as the training graph \mathcal{G}_T and the unseen graph \mathcal{G}_U , with a ratio of 80:20. The attacker is first trained on \mathcal{G}_T to learn the trigger generation strategy. Subsequently, a set of target nodes \mathcal{V}_B is selected from \mathcal{G}_T , and backdoor triggers are injected into these nodes to construct the backdoored training graph \mathcal{G}_B . The number of target nodes $|\mathcal{V}_B|$ is set to 40, 160, 160, and 565 for Cora, Pubmed, Flickr, and OGB-arxiv, respectively. To evaluate the attack effectiveness and defense performance under the inductive setting, nodes in \mathcal{G}_U are further divided into two equal-sized subsets. One subset is poisoned with the learned backdoor triggers and used to evaluate the attack success rate (ASR), while the remaining subset is kept clean and used to measure the clean accuracy (ACC). In addition to classification performance, we evaluate the ability of CoGBD to identify backdoors. Specifically, we report $\text{Recall}_{\text{tar}}$, the fraction of poisoned target nodes correctly detected, and $\text{Recall}_{\text{tri}}$, the fraction of trigger nodes correctly detected.

Implementation Details. For subgraph-based attacks, following [5, 35, 36], the trigger size is fixed to three nodes across all

datasets. For the feature-based attack SPEAR, following [7], the trigger dimension is set to $\max(0.02F, 5)$, where F denotes the dimension of node features. At the CoGBD detection stage, we set the suspicious ratio to $\rho = 3\%$ by default. During the noise-aware robust training stage, a two-layer GCN is used as the backbone classifier. The weight α and β are both chosen from $[2^{-4}, 2^{-3}, \dots, 2^4]$. The temperature parameter τ is varied from 0.1 to 1.0 in increments of 0.1, and the suppression strength λ is varied from 0.0 to 1.0 with the same step size. Each experiment is repeated five times with different random seeds, and we report the average performance. Full implementation details are provided in Appendix C.3.

6.2 Performance of Defense

Main Results. To answer **RQ1**, we compare CoGBD with representative defense methods across four datasets under both subgraph- and feature-based graph backdoor attacks. From the results summarized in Table 3 we draw two key observations: (1) CoGBD consistently achieves near-zero ASR across all datasets and attack types. In contrast, RIGBD is effective only against subgraph-based attacks and fails under feature-based GBAs. For instance, under SPEAR on OGB-arxiv, RIGBD yields an ASR of 96.61%, whereas CoGBD reduces the ASR to 0%. This advantage mainly stems from our consistency reconstruction model, which accurately identifies both poisoned target nodes and trigger nodes by capturing local node-neighborhood inconsistency, thereby enabling CoGBD to effectively defend against diverse backdoor triggers and attack paradigms. (2) CoGBD achieves clean accuracy comparable to, and in some cases slightly higher than, that of the vanilla GCN. This improvement is attributed to our noise-aware robust training objective, which assigns node weights based on reconstruction errors for both clean and suspicious nodes, thereby alleviating the impact of detection noise. Overall, these results show that CoGBD achieves strong backdoor defense performance across diverse attacks.

Additional Evaluation Results. More performance evaluations are deferred to the appendix due to space limitations, including clean-graph performance of CoGBD (Appendix D.1), robustness with different attack budgets (Appendix D.2), and transferability in different GNN backbones (Appendix D.5).

6.3 Ability to Detect Backdoors

To answer **RQ2**, we report in Table 4 the recall of poisoned target nodes ($\text{Recall}_{\text{tar}}$) and trigger nodes ($\text{Recall}_{\text{tri}}$) on OGB-arxiv, together with Clean ACC (trained on the clean graph), ASR, and ACC. From these results, we find that: (1) CoGBD consistently achieves over 80% recall on poisoned target nodes under both feature-based and subgraph-based attacks, highlighting the prevalence of feature-based homophily discrepancies induced by backdoor attacks and thereby supporting our theoretical insights. The effectiveness of CoGBD is particularly pronounced under feature-based GBAs, indicating that CoGBD effectively captures the most stealthy node-neighborhood inconsistencies introduced by feature-level perturbations. (2) CoGBD also demonstrates strong detection capability for trigger nodes under subgraph-based GBAs in most cases. For GTA and UGBA, the recall on trigger nodes reaches 100%; For DPGBA, the recall on trigger nodes is lower, as such triggers are designed to mimic in-distribution patterns and continue to mislead

Table 3: Results of backdoor defense.

Attacks	Defense	Cora		Pubmed		Flickr		OGB-arxiv	
		ASR(%)↓	ACC(%)↑	ASR(%)↓	ACC(%)↑	ASR(%)↓	ACC(%)↑	ASR(%)↓	ACC(%)↑
GTA	GCN	99.78	82.74	97.40	84.59	100.00	45.44	92.72	65.06
	GNNGuard	38.97	77.26	27.22	79.62	3.60	44.99	1.05	65.02
	RobustGCN	100.00	82.52	100.00	85.47	99.82	41.03	86.86	61.01
	RS	52.99	75.56	52.63	84.46	40.83	41.55	38.71	61.63
	ABL	31.37	81.19	50.68	84.51	0.00	41.18	45.19	64.12
	Prune	20.59	82.52	21.88	84.91	0.00	41.99	0.09	66.04
	OD	59.56	82.81	40.00	85.28	0.00	42.64	0.00	66.89
	RIGBD	9.74	84.74	2.30	84.56	0.00	44.51	0.00	62.74
	CoGBD	0.00	83.48	0.89	85.20	0.00	45.36	0.00	65.08
UGBA	GCN	99.63	82.15	99.52	85.13	98.83	43.61	99.14	65.51
	GNNGuard	28.41	77.41	19.95	80.02	0.00	43.88	78.65	66.43
	RobustGCN	88.19	82.37	94.14	85.48	92.32	40.70	94.93	61.19
	RS	49.30	76.96	50.55	84.40	27.43	41.27	27.05	60.62
	ABL	55.13	83.11	28.75	84.72	0.00	40.89	79.07	64.21
	Prune	97.34	82.00	100.00	85.21	98.95	41.82	92.73	63.79
	OD	0.00	83.33	23.45	84.93	0.00	41.20	0.04	65.01
	RIGBD	13.21	84.00	11.76	84.51	0.00	44.87	0.00	66.33
	CoGBD	0.00	84.30	1.12	84.33	0.00	44.36	2.88	65.42
DPGBA	GCN	96.61	82.37	99.03	83.62	99.98	44.14	96.75	65.06
	GNNGuard	89.37	78.07	96.08	81.73	92.85	44.57	96.79	65.07
	RobustGCN	97.56	80.22	97.57	84.97	100.00	41.43	96.58	65.10
	RS	51.73	74.89	64.62	82.99	97.31	42.10	47.01	60.14
	ABL	96.90	79.85	99.65	82.25	94.80	41.24	50.65	63.22
	Prune	20.81	80.44	40.71	84.39	91.67	43.78	0.16	63.45
	OD	94.10	81.78	99.59	84.37	99.29	44.53	96.86	64.70
	RIGBD	12.40	82.96	1.61	83.67	9.81	43.23	0.02	65.02
	CoGBD	0.00	84.67	0.00	85.47	0.00	43.19	0.06	65.98
SPEAR	GCN	97.27	84.07	92.84	84.91	100.00	44.33	96.56	66.90
	GNNGuard	52.55	79.63	70.12	81.48	44.86	44.29	97.51	67.82
	RobustGCN	90.77	81.41	91.45	85.54	100.00	40.80	95.99	61.37
	RS	85.61	76.22	87.10	84.68	96.78	41.23	83.31	61.19
	ABL	97.12	83.93	93.12	84.58	20.00	40.90	95.08	64.41
	Prune	99.56	81.85	95.38	85.00	95.89	42.01	98.91	65.65
	OD	99.41	83.63	90.01	85.41	90.39	40.70	72.55	66.17
	RIGBD	62.28	83.88	89.95	85.41	99.99	43.53	96.61	66.63
	CoGBD	0.00	83.41	7.27	84.76	0.00	43.62	0.00	67.23

Table 4: Results for the ability to detect backdoors.

Attacks	Clean ACC	ASR	ACC	Recall _{tar}	Recall _{tri}
GTA	65.17	0.00	65.08	100.00	100.00
UGBA	65.17	2.88	65.42	91.27	100.00
DPGBA	65.17	0.06	65.98	85.92	69.27
SPEAR	65.17	0.00	67.23	100.00	-

the model at test time. In this case, accurately identifying poisoned target nodes is more critical for suppressing ASR, and CoGBD effectively prioritizes target-node detection, which is sufficient to reduce the ASR to near zero despite partial trigger identification. Overall, these results demonstrate that CoGBD reliably identifies critical backdoor-related nodes, enabling effective mitigation across diverse

attack paradigms while preserving clean performance. Additional experiments on other datasets are provided in Appendix D.3.

6.4 Ablation Study

To answer **RQ3**, we compare the full CoGBD with four ablated variants: w/o $\mathcal{L}_{\text{node}}$, w/o $\mathcal{L}_{\text{neigh}}$, w/o $\mathcal{L}_{\text{homo}}$, and w/o $\mathcal{L}_{\text{noise}}$, which remove the node-level, neighborhood-level, feature-homophily reconstruction signals, and the noise-aware node weights, respectively. We evaluate all variants on OGB-arxiv under four representative attacks and report ASR and ACC in Table 5. From the table, we observe that: (1) Removing any reconstruction signal compromises the universality of the defense, preventing the model from achieving consistently low ASR across all attack types. Although

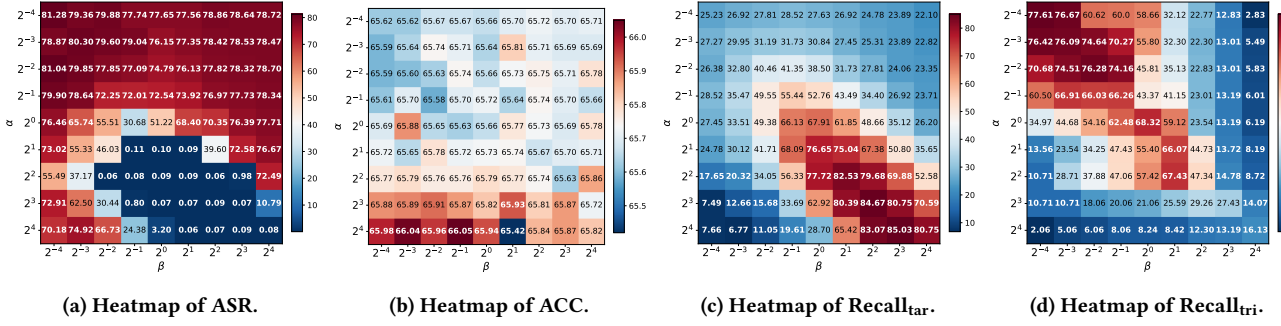
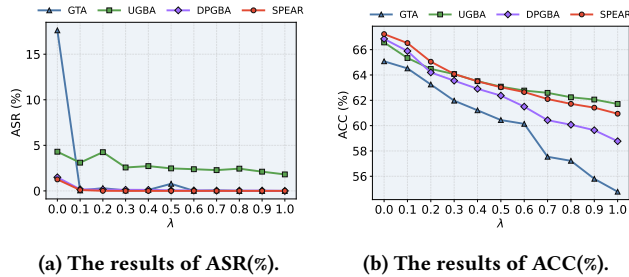
Figure 3: Sensitivity analysis of α and β .

Table 5: Ablation study on key components.

	GTA		UGBA		DPGBA		SPEAR	
	ASR	ACC	ASR	ACC	ASR	ACC	ASR	ACC
w/o $\mathcal{L}_{\text{node}}$	0.00	64.42	55.66	64.63	0.08	65.81	0.00	66.42
w/o $\mathcal{L}_{\text{neigh}}$	0.06	64.64	42.74	64.26	78.46	65.61	0.72	66.86
w/o $\mathcal{L}_{\text{homo}}$	23.00	64.51	54.16	64.66	79.31	65.67	0.00	66.31
w/o $\mathcal{L}_{\text{noise}}$	0.17	60.51	2.23	63.64	4.38	63.37	0.28	63.92
Ours	0.00	65.08	2.88	65.42	0.06	65.98	0.00	67.23

Figure 4: Sensitivity analysis of λ .

removing certain components remains effective for specific attacks (e.g., “w/o $\mathcal{L}_{\text{node}}$ ” on GTA, DPGBA, and SPEAR), as these attacks are more sensitive to neighborhood-level or cross-level inconsistencies, this behavior does not generalize to UGBA. This indicates that jointly modeling node-level, neighborhood-level, and feature-based homophily reconstruction signals is essential for capturing diverse GBA-induced inconsistencies and is necessary for achieving universal defense. (2) CoGBD consistently exhibits higher clean accuracy than “w/o $\mathcal{L}_{\text{noise}}$ ”. For instance, CoGBD improves clean accuracy by 4.57% and 3.31% over “w/o $\mathcal{L}_{\text{noise}}$ ” under GTA and SPEAR, respectively. Unlike “w/o $\mathcal{L}_{\text{noise}}$ ” variant, which treats all suspicious target nodes equally and is sensitive to detection noise, CoGBD incorporates noise-aware node weights into training, thereby mitigating noisy supervision and leading to more stable training.

6.5 Parameter Sensitivity Analysis

To answer RQ4, we conduct a sensitivity analysis of CoGBD with respect to α and β , which balance different reconstruction signals for consistency modeling, and λ , which controls the strength of suppressing suspicious nodes during noise-aware robust training.

Effect of α and β . We analyze the impact of the reconstruction weights α and β by varying them from 2^{-4} to 2^4 and evaluating CoGBD on OGB-arxiv under DPGBA, the most stealthy subgraph-based GBA. As shown in Fig. 3, increasing α and β steadily improves $\text{Recall}_{\text{tar}}$ while consistently reducing ASR. In particular, when $\alpha > 0$ and $\beta > 2^1$, CoGBD achieves near-zero ASR with strong clean accuracy. This indicates that, under DPGBA, emphasizing neighborhood-level and feature-based homophily reconstruction is more effective for identifying anomalous target nodes. Accurate detection of poisoned target nodes directly suppresses backdoor activation, leading to lower ASR and slightly improved ACC. Additional sensitivity results under feature-based GBA are provided in Appendix D.4.

Effect of λ . We study the effect of the suppression weight λ by varying it from 0 to 1.0 with a step size of 0.1, and evaluate CoGBD on OGB-arxiv under four representative attacks. Fig. 4 shows that increasing λ consistently reduces ASR while gradually lowering ACC, revealing a clear trade-off between backdoor suppression and clean performance. This trend arises because larger values of λ impose stronger unlearning on poisoned target nodes, effectively weakening trigger-induced patterns, but also amplify the impact of false positives, introducing training noise and degrading accuracy. Overall, $\lambda = 0.1$ provides a favorable balance in most cases, achieving low ASR while preserving high clean accuracy.

More Hyperparameters Analysis. We analyze the impact of more hyperparameters in Appendix D.4 due to the space limitation.

7 Conclusion

In this paper, we study a novel problem of universal graph backdoor defense. To bridge subgraph-based and feature-based attacks, we introduce a feature-based homophily perspective that characterizes node-neighborhood feature consistency. Through both theoretical analysis and empirical validation, we demonstrate that effective graph backdoor attacks consistently induce a distributional gap in feature-based homophily between clean nodes and backdoors. Building on this insight, we propose CoGBD, a consistency-guided framework for universal graph backdoor defense. By jointly modeling node-, neighborhood-, and cross-level consistency via multi-view reconstruction, CoGBD effectively identifies backdoors. Furthermore, a noise-aware robust training strategy mitigates the impact of detection uncertainty while eliminating trigger effects. Extensive experiments demonstrate that our method substantially reduces the attack success rate and preserves clean accuracy across both subgraph-based and feature-based graph backdoor attacks.

References

- [1] Peter W Battaglia, Jessica B Hamrick, Victor Bapst, Alvaro Sanchez-Gonzalez, Vinicius Zambaldi, Mateusz Malinowski, Andrea Tacchetti, David Raposo, Adam Santoro, Ryan Faulkner, et al. 2018. Relational inductive biases, deep learning, and graph networks. *arXiv preprint arXiv:1806.01261* (2018).
- [2] Pietro Bongini, Monica Bianchini, and Franco Scarselli. 2021. Molecular generative graph neural networks for drug discovery. *Neurocomputing* 450 (2021), 242–252.
- [3] Xinyun Chen, Chang Liu, Bo Li, Kimberly Lu, and Dawn Song. 2017. Targeted backdoor attacks on deep learning systems using data poisoning. *arXiv preprint arXiv:1712.05526* (2017).
- [4] Yang Chen, Zhonglin Ye, Haixing Zhao, Ying Wang, and Subrata Kumar Sarker. 2023. Feature-Based Graph Backdoor Attack in the Node Classification Task. *Int. J. Intell. Syst.* 2023 (Jan. 2023), 13 pages.
- [5] Enyan Dai, Minhua Lin, Xiang Zhang, and Suhang Wang. 2023. Unnoticeable backdoor attacks on graph neural networks. In *Proceedings of the ACM Web Conference 2023*. 2263–2273.
- [6] Kaize Ding, Jundong Li, Rohit Bhanushali, and Huan Liu. 2019. Deep Anomaly Detection on Attributed Networks. In *Proceedings of the 2019 SIAM International Conference on Data Mining (SDM)*. 594–602.
- [7] Yuanhao Ding, Yang Liu, Yugang Ji, Weigao Wen, Qing He, and Xiang Ao. 2025. SPEAR: A Structure-Preserving Manipulation Method for Graph Backdoor Attacks. In *Proceedings of the ACM on Web Conference 2025 (WWW '25)*. 1237–1247.
- [8] Wenqi Fan, Yao Ma, Qing Li, Yuan He, Eric Zhao, Jiliang Tang, and Dawei Yin. 2019. Graph neural networks for social recommendation. In *The world wide web conference*. 417–426.
- [9] Tianyu Gu, Kang Liu, Brendan Dolan-Gavitt, and Siddharth Garg. 2019. BadNets: Evaluating Backdooring Attacks on Deep Neural Networks. *IEEE Access* 7 (2019), 47230–47244.
- [10] Will Hamilton, Zhitao Ying, and Jure Leskovec. 2017. Inductive representation learning on large graphs. *Advances in neural information processing systems* 30 (2017).
- [11] Weihua Hu, Matthias Fey, Marinka Zitnik, Yuxiao Dong, Hongyu Ren, Bowen Liu, Michele Catasta, and Jure Leskovec. 2020. Open graph benchmark: Datasets for machine learning on graphs. *Advances in neural information processing systems* 33 (2020), 22118–22133.
- [12] Thomas N. Kipf and Max Welling. 2017. Semi-Supervised Classification with Graph Convolutional Networks. In *5th International Conference on Learning Representations, ICLR 2017, Toulon, France, April 24–26, 2017, Conference Track Proceedings*. OpenReview.net.
- [13] Sanjay Kumar, Abhishek Mallik, Anavi Khetarpal, and B.S. Panda. 2022. Influence maximization in social networks using graph embedding and graph neural network. *Information Sciences* 607 (2022), 1617–1636.
- [14] Fan Li, Xiaoyang Wang, Dawei Cheng, Wenjie Zhang, Chen Chen, Ying Zhang, and Xuemin Lin. 2025. Tegu: Data-centric graph unlearning based on transferable condensation. *IEEE Transactions on Knowledge and Data Engineering* 38, 2 (2025), 1334–1348.
- [15] Fan Li, Zhiyu Xu, Dawei Cheng, and Xiaoyang Wang. 2024. AdaRisk: risk-adaptive deep reinforcement learning for vulnerable nodes detection. *IEEE Transactions on Knowledge and Data Engineering* 36, 11 (2024), 5576–5590.
- [16] Jiangtong Li, Dungy Liu, Dawei Cheng, and Changchun Jiang. 2024. Attack by Yourself: Effective and Unnoticeable Multi-Category Graph Backdoor Attacks with Subgraph Triggers Pool. *arXiv preprint arXiv:2412.17213* (2024).
- [17] Yiming Li, Yong Jiang, Zhifeng Li, and Shu-Tao Xia. 2022. Backdoor learning: A survey. *IEEE transactions on neural networks and learning systems* 35, 1 (2022), 5–22.
- [18] Yige Li, Xixiang Lyu, Nodens Koren, Lingjuan Lyu, Bo Li, and Xingjun Ma. 2021. Anti-backdoor learning: Training clean models on poisoned data. *Advances in Neural Information Processing Systems* 34 (2021), 14900–14912.
- [19] Yixin Liu, Yizhen Zheng, Daokun Zhang, Vincent CS Lee, and Shirui Pan. 2023. Beyond smoothing: Unsupervised graph representation learning with edge heterophily discriminating. In *Proceedings of the AAAI conference on artificial intelligence*, Vol. 37. 4516–4524.
- [20] Fanchao Qi, Yangyi Chen, Mukai Li, Yuan Yao, Zhiyuan Liu, and Maosong Sun. 2021. Onion: A simple and effective defense against textual backdoor attacks. In *Proceedings of the 2021 conference on empirical methods in natural language processing*. 9558–9566.
- [21] Fanchao Qi, Mukai Li, Yangyi Chen, Zhengyan Zhang, Zhiyuan Liu, Yasheng Wang, and Maosong Sun. 2021. Hidden Killer: Invisible Textual Backdoor Attacks with Syntactic Trigger. In *Annual Meeting of the Association for Computational Linguistics*. <https://api.semanticscholar.org/CorpusID:235196099>
- [22] Pedro Quesado, Luis HM Torres, Bernardete Ribeiro, and Joel P Arrais. 2024. A hybrid gnn approach for improved molecular property prediction. *Journal of Computational Biology* 31, 11 (2024), 1146–1157.
- [23] Prithviraj Sen, Galileo Namata, Mustafa Bilgic, Lise Getoor, Brian Galligher, and Tina Eliassi-Rad. 2008. Collective Classification in Network Data. *AI Magazine* 29, 3 (Sep. 2008), 93.
- [24] Petar Veličković, Guillem Cucurull, Arantxa Casanova, Adriana Romero, Pietro Lio, and Yoshua Bengio. 2018. Graph attention networks. In *ICLR*.
- [25] Binghui Wang, Jinyuan Jia, Xiaoyu Cao, and Neil Zhenqiang Gong. 2021. Certified robustness of graph neural networks against adversarial structural perturbation. In *Proceedings of the 27th ACM SIGKDD Conference on Knowledge Discovery & Data Mining*. 1645–1653.
- [26] Kaiyang Wang, Huaxin Deng, Yijia Xu, Zhonglin Liu, and Yong Fang. 2024. Multi-target label backdoor attacks on graph neural networks. *Pattern Recognition* 152 (2024), 110449.
- [27] Zonghan Wu, Shirui Pan, Fengwen Chen, Guodong Long, Chengqi Zhang, and Philip S Yu. 2020. A comprehensive survey on graph neural networks. *IEEE transactions on neural networks and learning systems* 32, 1 (2020), 4–24.
- [28] Zonghan Wu, Shirui Pan, Fengwen Chen, Guodong Long, Chengqi Zhang, and Philip S Yu. 2020. A comprehensive survey on graph neural networks. *IEEE transactions on neural networks and learning systems* 32, 1 (2020), 4–24.
- [29] Zhaohan Xi, Ren Pang, Shouling Ji, and Ting Wang. 2021. Graph backdoor. In *30th USENIX security symposium (USENIX Security 21)*. 1523–1540.
- [30] Hui Xia, Xiangwei Zhao, Rui Zhang, Shuo Xu, and Luming Wang. 2025. Clean-label graph backdoor attack in the node classification task. In *Proceedings of the Thirty-Ninth AAAI Conference on Artificial Intelligence and Thirty-Seventh Conference on Innovative Applications of Artificial Intelligence and Fifteenth Symposium on Educational Advances in Artificial Intelligence (AAAI'25/IAAI'25/EAAI'25)*. AAAI Press, Article 2412, 9 pages.
- [31] Jing Xu and Stjepan Picek. 2022. Poster: Clean-label Backdoor Attack on Graph Neural Networks. In *Proceedings of the 2022 ACM SIGSAC Conference on Computer and Communications Security (Los Angeles, CA, USA) (CCS '22)*. Association for Computing Machinery, New York, NY, USA, 3491–3493.
- [32] Hanqing Zeng, Hongkuan Zhou, Ajitesh Srivastava, Rajgopal Kannan, and Viktor Prasanna. 2019. Graphsaint: Graph sampling based inductive learning method. *arXiv preprint arXiv:1907.04931* (2019).
- [33] Xiang Zhang and Marinka Zitnik. 2020. Gnn-guard: Defending graph neural networks against adversarial attacks. *Advances in neural information processing systems* 33 (2020), 9263–9275.
- [34] Zaixi Zhang, Jinyuan Jia, Binghui Wang, and Neil Zhenqiang Gong. 2021. Backdoor attacks to graph neural networks. In *Proceedings of the 26th ACM symposium on access control models and technologies*. 15–26.
- [35] Zhiwei Zhang, Minhua Lin, Enyan Dai, and Suhang Wang. 2024. Rethinking graph backdoor attacks: A distribution-preserving perspective. In *Proceedings of the 30th ACM SIGKDD Conference on Knowledge Discovery and Data Mining*. 4386–4397.
- [36] Zhiwei Zhang, Minhua Lin, Junjie Xu, Zongyu Wu, Enyan Dai, and Suhang Wang. 2025. Robustness Inspired Graph Backdoor Defense. In *International Conference on Learning Representations*, Y. Yue, A. Garg, N. Peng, F. Sha, and R. Yu (Eds.), Vol. 2025. 1958–1984.
- [37] Haibin Zheng, Haiyang Xiong, Jinyin Chen, Haonan Ma, and Guohan Huang. 2024. Motif-Backdoor: Rethinking the Backdoor Attack on Graph Neural Networks via Motifs. *IEEE Transactions on Computational Social Systems* 11, 2 (2024), 2479–2493.
- [38] Jie Zhou, Ganqu Cui, Shengding Hu, Zhengyan Zhang, Cheng Yang, Zhiyuan Liu, Lifeng Wang, Changcheng Li, and Maosong Sun. 2020. Graph neural networks: A review of methods and applications. *AI open* 1 (2020), 57–81.
- [39] Dingyuan Zhu, Ziwei Zhang, Peng Cui, and Wenwu Zhu. 2019. Robust Graph Convolutional Networks Against Adversarial Attacks. In *Proceedings of the 25th ACM SIGKDD International Conference on Knowledge Discovery & Data Mining (KDD '19)*. 1399–1407.
- [40] Xiaoqian Zhu, Xiang Ao, Zidi Qin, Yanpeng Chang, Yang Liu, Qing He, and Jianping Li. 2021. Intelligent financial fraud detection practices in post-pandemic era. *The Innovation* 2, 4 (2021), 100176.

Appendix

A Detailed Proofs

Setup. For analytical clarity, we consider an L -layer linear GNN with normalized adjacency matrix $\bar{\mathbf{A}}$. Let $\mathbf{H}^{(l)}$ denote the node representations after the l -th message-passing layer, given by $\mathbf{H}^{(l)} = \bar{\mathbf{A}}^l \mathbf{X}$, and let the final logits be $\mathbf{Z} = \mathbf{H}^{(l)} \mathbf{W}$. For a node v , its l -layer representation is denoted by $h_v^{(l)} \triangleq [\mathbf{H}^{(l)}]_v$.

A.1 Proof of Lemma 1

LEMMA 1. Let $h_v^{(l)}$ and $h'_v{}^{(l)}$ denote the l -th layer representations of a target node v on the clean and backdoored graphs \mathcal{G}_T and \mathcal{G}_B , respectively. We further denote $\pi_{vu}^{(l)} \triangleq (\bar{\mathbf{A}}^l)_{vu}$, $\pi'_{vu}{}^{(l)} \triangleq ((\bar{\mathbf{A}} + \Delta\bar{\mathbf{A}})^l)_{vu}$. Then, the representation shift $\Delta h_v^{(l)} \triangleq h'_v{}^{(l)} - h_v^{(l)}$ can be written as:

$$\Delta h_v^{(l)} = \sum_{u \in \mathcal{V}} (\pi'_{vu}{}^{(l)} - \pi_{vu}^{(l)}) x_u + \sum_{u \in \mathcal{V}} \pi'_{vu}{}^{(l)} \Delta x_u,$$

where x_u is the original feature vector of node u and Δx_u denotes the feature perturbation applied on node u .

PROOF. On the clean training graph \mathcal{G}_T , the l -layer representation of node v is given by:

$$h_v^{(l)} = [\bar{\mathbf{A}}^l \mathbf{X}]_v = \sum_{u \in \mathcal{V}} (\bar{\mathbf{A}}^l)_{vu} x_u = \sum_{u \in \mathcal{V}} \pi_{vu}^{(l)} x_u. \quad (12)$$

On the backdoored graph \mathcal{G}_B , the representation becomes:

$$\begin{aligned} h'_v{}^{(l)} &= [(\bar{\mathbf{A}} + \Delta\bar{\mathbf{A}})^l (\mathbf{X} + \Delta\mathbf{X})]_v \\ &= \sum_{u \in \mathcal{V}} ((\bar{\mathbf{A}} + \Delta\bar{\mathbf{A}})^l)_{vu} (x_u + \Delta x_u) = \sum_{u \in \mathcal{V}} \pi'_{vu}{}^{(l)} (x_u + \Delta x_u). \end{aligned} \quad (13)$$

Subtracting (12) from (13) yields:

$$\Delta h_v^{(l)} \triangleq h'_v{}^{(l)} - h_v^{(l)} = \sum_{u \in \mathcal{V}} (\pi'_{vu}{}^{(l)} - \pi_{vu}^{(l)}) x_u + \sum_{u \in \mathcal{V}} \pi'_{vu}{}^{(l)} \Delta x_u, \quad (14)$$

which completes the proof. \square

A.2 Proof of Lemma 2

LEMMA 2. Consider a targeted graph backdoor attack on node v with target class y_t . The GNN classifier produces logits $z_{v,c} = \mathbf{w}_c^\top h_v^{(l)}$, where \mathbf{w}_c is the class-specific weight vector. The predicted probability for class c is $p_{v,c} = \frac{\exp(z_{v,c})}{\sum_{c'} \exp(z_{v,c'})}$. Let $\ell_{\text{CE}}(v) = -\log p_{v,y_t}$ be the target-class cross-entropy loss. For a small representation shift $\Delta h_v^{(l)}$ induced by the trigger, a necessary condition for decreasing $\ell_{\text{CE}}(v)$ is:

$$\langle \mathbf{w}_{y_t} - \bar{\mathbf{w}}_v, \Delta h_v^{(l)} \rangle > 0,$$

where $\bar{\mathbf{w}}_v \triangleq \sum_c p_{v,c} \mathbf{w}_c$ denotes the expected classifier weight under the current predictive distribution of node v .

PROOF. We derive a first-order necessary condition under which a backdoor trigger can decrease the target-class loss of node v . Assume a linear classifier on top of the l -layer representation $h_v^{(l)}$. The logit for class c is given by $z_{v,c} = \mathbf{w}_c^\top h_v^{(l)}$, and the predictive distribution follows the softmax $p_{v,c} = \exp(z_{v,c}) / \sum_{c'} \exp(z_{v,c'})$. The attack objective is to increase the confidence on the target class y_t , which is equivalent to reducing the cross-entropy loss:

$$\ell_{\text{CE}}(v) = -\log p_{v,y_t}. \quad (15)$$

We first compute the gradient of $\ell_{\text{CE}}(v)$ with respect to $h_v^{(l)}$. By the chain rule, we have:

$$\frac{\partial \ell_{\text{CE}}(v)}{\partial h_v^{(l)}} = \sum_c \frac{\partial \ell_{\text{CE}}(v)}{\partial z_{v,c}} \frac{\partial z_{v,c}}{\partial h_v^{(l)}}. \quad (16)$$

Since $\ell_{\text{CE}}(v) = -\log p_{v,y_t}$, it follows that $\frac{\partial \ell_{\text{CE}}(v)}{\partial p_{v,k}} = -\frac{1}{p_{v,y_t}} \mathbb{1}[k = y_t]$. Moreover, the Jacobian of the softmax satisfies $\frac{\partial p_{v,k}}{\partial z_{v,c}} = p_{v,k} (\mathbb{1}[k = c] - p_{v,c})$. Combining the above relations yields:

$$\frac{\partial \ell_{\text{CE}}(v)}{\partial z_{v,c}} = \sum_k \frac{\partial \ell_{\text{CE}}(v)}{\partial p_{v,k}} \frac{\partial p_{v,k}}{\partial z_{v,c}} = p_{v,c} - \mathbb{1}[c = y_t]. \quad (17)$$

Noting that $\frac{\partial z_{v,c}}{\partial h_v^{(l)}} = \mathbf{w}_c$, substituting this result into Eq. (16) gives:

$$\frac{\partial \ell_{\text{CE}}(v)}{\partial h_v^{(l)}} = \sum_c (p_{v,c} - \mathbb{1}[c = y_t]) \mathbf{w}_c = \sum_c p_{v,c} \mathbf{w}_c - \mathbf{w}_{y_t} = \bar{\mathbf{w}}_v - \mathbf{w}_{y_t}, \quad (18)$$

where $\bar{\mathbf{w}}_v \triangleq \sum_c p_{v,c} \mathbf{w}_c$. Let $\Delta h_v^{(l)}$ denote the representation shift induced by the trigger, and define:

$$\Delta \ell_{\text{CE}}(v) \triangleq \ell_{\text{CE}}(h_v^{(l)} + \Delta h_v^{(l)}) - \ell_{\text{CE}}(h_v^{(l)}). \quad (19)$$

By the first-order Taylor expansion of $\ell_{\text{CE}}(\cdot)$ around $h_v^{(l)}$, we obtain:

$$\ell_{\text{CE}}(h_v^{(l)} + \Delta h_v^{(l)}) = \ell_{\text{CE}}(h_v^{(l)}) + \langle \nabla_{h_v^{(l)}} \ell_{\text{CE}}(v), \Delta h_v^{(l)} \rangle + o(\|\Delta h_v^{(l)}\|), \quad (20)$$

and therefore:

$$\Delta \ell_{\text{CE}}(v) = \langle \nabla_{h_v^{(l)}} \ell_{\text{CE}}(v), \Delta h_v^{(l)} \rangle + o(\|\Delta h_v^{(l)}\|) \approx \langle \bar{\mathbf{w}}_v - \mathbf{w}_{y_t}, \Delta h_v^{(l)} \rangle. \quad (21)$$

For an effective targeted attack, the target-class loss must decrease, i.e., $\Delta \ell_{\text{CE}}(v) < 0$. Ignoring higher-order terms then yields the first-order necessary condition:

$$\langle \mathbf{w}_{y_t} - \bar{\mathbf{w}}_v, \Delta h_v^{(l)} \rangle > 0, \quad (22)$$

which completes the proof. \square

A.3 Proof of Theorem 1

Setup. For clarity, we instantiate AGGR as mean aggregation and $\text{sim}(\cdot, \cdot)$ as the inner product. For each node v , define its neighborhood mean feature $m_v \triangleq \frac{1}{|N(v)|} \sum_{u \in N(v)} x_u$, and the feature-based homophily as $\mathcal{H}_{\text{feat}}(v) = \langle x_v, m_v \rangle$.

THEOREM 1. Given a backdoored graph \mathcal{G}_B with clean node set \mathcal{V}_C and backdoored node set \mathcal{V}_B . For any effective graph backdoor attack, the expected feature-based homophily of backdoored nodes is lower than that of clean nodes:

$$\mathbb{E}_{v \sim \mathcal{V}_B} [\mathcal{H}_{\text{feat}}(v)] < \mathbb{E}_{v \sim \mathcal{V}_C} [\mathcal{H}_{\text{feat}}(v)].$$

PROOF. To prove that effective graph backdoor attacks necessarily introduce a systematic discrepancy in feature-based homophily between clean and backdoored nodes, We state two mild regularity assumptions that capture the typical behavior of clean nodes and the geometric requirement of targeted attacks.

Key assumption (clean-majority regularity). Clean nodes constitute the majority and follow a relatively stable local pattern, i.e.,

$$\mathbb{E}_{v \sim \mathcal{V}_C} [\mathcal{H}_{\text{feat}}(v)] \geq \mu, \quad (23)$$

where μ denotes the mean feature-based homophily over the whole graph.

Key assumption (target direction is locally misaligned). Next, recall from Lemma 2 that an effective targeted attack requires the induced representation shift to align with the target-aware direction

$$\mathbf{g}_v \triangleq \mathbf{w}_{y_t} - \bar{\mathbf{w}}_v, \quad \langle \mathbf{g}_v, \Delta h_v^{(l)} \rangle > 0. \quad (24)$$

For poisoned nodes, pushing representations along \mathbf{g}_v is generally not aligned with their original neighborhood semantics; we assume this misalignment holds in expectation:

$$\mathbb{E}_{v \sim \mathcal{V}_B} [\langle \mathbf{g}_v, m_v \rangle] \leq -\gamma, \quad \gamma > 0. \quad (25)$$

We now analyze how an effective attack that satisfies (24) affects $\mathcal{H}_{\text{feat}}(v)$.

Case I: feature-based GBA ($\Delta \bar{\mathbf{A}} = \mathbf{0}$). Feature-based attacks modify node attributes while keeping the neighborhood structure unchanged. In this case, Lemma 1 reduces to:

$$\Delta h_v^{(l)} = \sum_{u \in \mathcal{V}} \pi_{vu}^{(l)} \Delta x_u, \quad \pi_{vu}^{(l)} = (\bar{\mathbf{A}}^l)_{vu}, \quad (26)$$

since $\pi_{vu}'^{(l)} = \pi_{vu}^{(l)}$. An effective attack requires $\langle \mathbf{g}_v, \Delta h_v^{(l)} \rangle > 0$; a canonical way to satisfy this condition is to inject a perturbation component that is positively correlated with \mathbf{g}_v (e.g., concentrating Δx_u on $u = v$ and choosing Δx_v to have $\langle \mathbf{g}_v, \Delta x_v \rangle > 0$). Under mean aggregation, the neighborhood mean m_v is unchanged by feature-only attacks, and thus:

$$\mathcal{H}_{\text{feat}}(v) = \langle x_v + \Delta x_v, m_v \rangle = \langle x_v, m_v \rangle + \langle \Delta x_v, m_v \rangle. \quad (27)$$

For effective targeted perturbations, Δx_v necessarily contains a component aligned with \mathbf{g}_v , i.e., $\Delta x_v = \lambda \mathbf{g}_v + r_v$ with $\lambda > 0$ and $\langle \mathbf{g}_v, r_v \rangle = 0$. Substituting into (27) gives:

$$\mathcal{H}_{\text{feat}}(v) = \langle x_v, m_v \rangle + \lambda \langle \mathbf{g}_v, m_v \rangle + \langle r_v, m_v \rangle. \quad (28)$$

Taking expectation over $v \sim \mathcal{V}_B$ and using (25) yields:

$$\mathbb{E}_{v \sim \mathcal{V}_B} [\mathcal{H}_{\text{feat}}(v)] \leq \mathbb{E}_{v \sim \mathcal{V}_B} [\langle x_v, m_v \rangle] - \lambda \gamma + \mathbb{E}_{v \sim \mathcal{V}_B} [\langle r_v, m_v \rangle]. \quad (29)$$

Since r_v does not contribute to satisfying the attack condition (24), a rational adversary that prioritizes attack effectiveness has no incentive to choose r_v to systematically increase $\langle r_v, m_v \rangle$. Accordingly, in the worst case we assume $\mathbb{E}[\langle r_v, m_v \rangle] \leq 0$, which implies a strict drop by $\lambda \gamma$ in expectation.

Case II: subgraph-based GBA ($\Delta X = \mathbf{0}$). Subgraph-based attacks alter the neighborhood structure of v while keeping x_v unchanged. In this case, Lemma 1 reduces to the structure-driven term:

$$\Delta h_v^{(l)} = \sum_{u \in \mathcal{V}} (\pi_{vu}'^{(l)} - \pi_{vu}^{(l)}) x_u, \quad \pi_{vu}'^{(l)} = ((\bar{\mathbf{A}} + \Delta \bar{\mathbf{A}})^l)_{vu}, \quad (30)$$

which shows that subgraph-based attacks act by reweighting the aggregation toward selected nodes. Let m_v denote the post-attack neighborhood mean under mean aggregation. Since the attack is effective, it must satisfy (24), which in this case is achieved by shifting aggregation weights so that $\Delta h_v^{(l)}$ has positive correlation with \mathbf{g}_v . Such reweighting inevitably drifts the neighborhood mean away from the original neighborhood semantics of v and decreases $\langle x_v, m_v \rangle$ in expectation; we assume that this effect holds with a non-trivial margin:

$$\mathbb{E}_{v \sim \mathcal{V}_B} [\langle x_v, m_v \rangle] \leq \mathbb{E}_{v \sim \mathcal{V}_B} [\langle x_v, m_v^{\text{clean}} \rangle] - \gamma', \quad \gamma' > 0, \quad (31)$$

where m_v^{clean} denotes the neighborhood mean before injecting trigger edges/subgraphs. Therefore, subgraph-based attacks also induce a strict decrease in feature-based homophily on poisoned nodes in expectation.

Combining both cases, effective GBAs reduce $\mathbb{E}_{v \sim \mathcal{V}_B} [\mathcal{H}_{\text{feat}}(v)]$ by a non-trivial margin, whereas clean nodes preserve a stable homophily level as in (23). Consequently,

$$\mathbb{E}_{v \sim \mathcal{V}_B} [\mathcal{H}_{\text{feat}}(v)] < \mathbb{E}_{v \sim \mathcal{V}_C} [\mathcal{H}_{\text{feat}}(v)],$$

which proves Theorem 1. \square

A.4 Feature-based Homophily on Trigger Nodes

In this section, we further discuss why trigger nodes also tend to exhibit a feature-based homophily gap on the backdoored graph. Our goal is to explain a common phenomenon observed across diverse subgraph-based GBAs:

$$\mathbb{E}_{v \sim \mathcal{V}_{\text{tri}}} [\mathcal{H}_{\text{feat}}(v)] < \mathbb{E}_{v \sim \mathcal{V}_C} [\mathcal{H}_{\text{feat}}(v)], \quad (32)$$

where \mathcal{V}_{tri} denotes the trigger-node set. We first categorize subgraph-based trigger generators according to whether they impose an explicit feature-similarity constraint on trigger nodes. Specifically, we consider: (i) unconstrained triggers, such as GTA [29] and DPGBA [35], where trigger nodes are generated primarily for attack activation without explicitly enforcing consistency between a trigger node and its post-attachment neighborhood; and (ii) similarity-constrained triggers, such as UGBA [5], where trigger nodes are encouraged to resemble the attached poisoned target node in feature space. We show that unconstrained generators typically induce a pronounced homophily gap on trigger nodes, while similarity constraints can narrow but generally do not eliminate the gap due to the mixed neighborhood context after attachment.

Setup. Following Sec. A.3, we instantiate AGGR as mean aggregation and $\text{sim}(\cdot, \cdot)$ as the inner product. For each node v , define the neighborhood mean $m_v \triangleq \frac{1}{|\mathcal{N}(v)|} \sum_{u \in \mathcal{N}(v)} x_u$ and $\mathcal{H}_{\text{feat}}(v) = \langle x_v, m_v \rangle$. For a trigger node $v_t \in \mathcal{V}_{\text{tri}}$, its post-attachment neighborhood typically contains a mixture of (i) poisoned targets that the trigger connects to and (ii) other trigger nodes inside the injected subgraph. Accordingly, we decompose the post-attachment neighborhood mean as:

$$m_{v_t} = \alpha_t \bar{x}_{\text{tar}}(v_t) + \alpha_r \bar{x}_{\text{tri}}(v_t) + \alpha_o \bar{x}_{\text{oth}}(v_t), \quad \alpha_t + \alpha_r + \alpha_o = 1, \quad (33)$$

where $\bar{x}_{\text{tar}}(v_t)$, $\bar{x}_{\text{tri}}(v_t)$, and $\bar{x}_{\text{oth}}(v_t)$ are the mean features of target neighbors, trigger neighbors, and other neighbors of v_t , respectively, and $\alpha_{\{\cdot\}}$ are the corresponding neighborhood proportions. Then

$$\mathcal{H}_{\text{feat}}(v_t) = \alpha_t \langle x_{v_t}, \bar{x}_{\text{tar}}(v_t) \rangle + \alpha_r \langle x_{v_t}, \bar{x}_{\text{tri}}(v_t) \rangle + \alpha_o \langle x_{v_t}, \bar{x}_{\text{oth}}(v_t) \rangle. \quad (34)$$

Eq. (34) highlights that improving the similarity between a trigger node and the attached poisoned target only directly affects the first term, while the overall homophily also depends on how x_{v_t} aligns with the remaining mixed neighborhood context.

Unconstrained trigger generators. For unconstrained triggers, the trigger generator does not explicitly enforce that each trigger node remains consistent with its post-attachment neighborhood mean m_{v_t} . In such cases, the neighborhood of a trigger node is often dominated by other trigger nodes (i.e., α_r is large) and only weakly anchored to a small set of attached poisoned targets (small

α_t). Since the injected subgraph is engineered for attack activation rather than local semantic regularity, trigger nodes are not explicitly optimized to align with their surrounding trigger-induced context. Accordingly, we assume that the average feature consistency among trigger nodes inside the injected subgraph is bounded by a constant:

$$\mathbb{E}_{v_t \sim \mathcal{V}_{\text{tri}}}[\langle x_{v_t}, \bar{x}_{\text{tri}}(v_t) \rangle] \leq \rho, \quad (35)$$

where ρ is generally lower than the homophily level observed on clean neighborhoods. Combined with the mixed neighborhood composition in Eq. (34), this bound implies that the overall feature-based homophily $\mathcal{H}_{\text{feat}}(v_t)$ of trigger nodes is reduced in expectation, leading to a pronounced homophily gap as in Eq. (32).

Similarity-constrained trigger generators. Some attacks additionally enforce a feature-similarity constraint between each trigger node v_t and its attached target v_p , which can be written as:

$$\mathcal{L}_{\text{sim}} = \sum_{(v_t, v_p) \in \mathcal{E}_{\text{attach}}} \ell_{\text{sim}}(\langle x_{v_t}, x_{v_p} \rangle), \quad (36)$$

where $\ell_{\text{sim}}(\cdot)$ is a monotonically decreasing penalty (e.g., a hinge loss). Minimizing \mathcal{L}_{sim} directly increases $\langle x_{v_t}, x_{v_p} \rangle$ and thus improves the first term in Eq. (34). This effect explains why similarity-constrained triggers are typically more “stealthy” at the attachment point and can narrow the trigger-node homophily gap.

However, Eq. (36) does not directly control the remaining terms in Eq. (34). In particular, when α_t is small (i.e., the neighborhood of v_t is dominated by other trigger nodes), improving $\langle x_{v_t}, x_{v_p} \rangle$ can only increase $\mathcal{H}_{\text{feat}}(v_t)$ proportionally to α_t . Under feature normalization (so that $|\langle x_{v_t}, \cdot \rangle| \leq 1$), we have the crude bound:

$$\mathcal{H}_{\text{feat}}(v_t) \leq \alpha_t + (1 - \alpha_t) \cdot \max\{\langle x_{v_t}, \bar{x}_{\text{tri}}(v_t) \rangle, \langle x_{v_t}, \bar{x}_{\text{oth}}(v_t) \rangle\}, \quad (37)$$

which makes explicit that the similarity constraint can narrow but may not eliminate the gap unless the generator also enforces node-neighborhood consistency with respect to the entire mixed context (i.e., all terms in Eq. (34)). This reveals an inherent trade-off: increasing stealthiness by making trigger nodes similar to attached targets does not guarantee high homophily once the trigger is embedded into a mixed trigger-target neighborhood optimized for attack activation.

Empirical validation. Table 1 reports the average feature-based homophily of clean nodes, poisoned targets, and trigger nodes computed on the backdoored graph. Across datasets, we observe that trigger nodes produced by unconstrained generators (i.e., GTA [29] and DPGBA [35]) exhibit a clear drop in $\mathcal{H}_{\text{feat}}$ compared with clean nodes, consistent with Eq. (32). Similarity-constrained generators (i.e., UGBA [5]) yield trigger nodes whose homophily is closer to that of clean nodes, indicating that the constraint in Eq. (36) indeed narrows the gap; nevertheless, trigger-node homophily remains consistently below the clean baseline. Overall, these results support our insight that feature-based homophily provides a stable signal for exposing trigger nodes under diverse subgraph-based GBAs.

B Algorithm and Complexity

B.1 Training Algorithm

Algorithm 1 summarizes the training procedure of CoGBD, which consists of two stages. **Stage I: Detection of Consistency Deviation (lines 1–11).** We first pretrain a consistency reconstruction

Algorithm 1: Algorithm of CoGBD

Input: Backdoored training graph $\mathcal{G}_B = (\mathcal{V}'_T, \mathcal{E}'_T, \mathcal{X}'_T)$; suspicious ratio ρ ; loss weights α, β ; temperature parameter τ ; suppression strength λ .
Output: Backdoor-robust GNN classifier f_g .

- 1 **Stage I: Identifying Backdoors**
 - 2 Initialize parameters θ_{rec} of the consistency reconstruction model (encoder f_{enc} and decoders $f_{\text{dec}}^x, f_{\text{dec}}^m$);
 - 3 **while not converged do**
 - 4 Update θ_{rec} by minimizing the overall reconstruction objective \mathcal{L}_{rec} in Eq. (6) on \mathcal{G}_B ;
 - 5 **end**
 - 6 **foreach** $v_i \in \mathcal{V}'_T$ **do**
 - 7 Compute reconstruction error e_i using Eq. (7);
 - 8 **end**
 - 9 Select the top $\rho\%$ nodes with largest e_i as the backdoors set;
 - 10 Partition the backdoors set into: suspicious trigger nodes (unlabeled) and suspicious target nodes \mathcal{V}_S (labeled);
 - 11 Remove edges incident to suspicious trigger nodes from \mathcal{G}_B ;
 - 12 **Stage II: Noise-aware Robust Training**
 - 13 Initialize parameters θ_g of an l -layer GNN classifier f_g ;
 - 14 **while not converged do**
 - 15 Update θ_g by minimizing the noise-aware robust objective $\mathcal{L}_{\text{noise}}$ in Eq. (11);
 - 16 **end**
 - 17 **return** Backdoor-robust GNN classifier f_g ;
-

model on the backdoored training graph \mathcal{G}_B (lines 2–5). Specifically, the encoder and decoders are optimized by minimizing the tri-signal reconstruction objective in Eq. (6), which captures graph consistency from node-level, neighborhood-level, and feature-based homophily. After convergence, we compute the reconstruction error e_i for each node and select the top $\rho\%$ nodes as abnormal. These nodes are further partitioned into suspicious trigger nodes (unlabeled) and suspicious target nodes (labeled). Edges incident to suspicious trigger nodes are removed from the training graph, while suspicious target nodes are retained for soft suppression in training. **Stage II: Noise-aware Robust Training (lines 12–16).** We then initialize a L -layer GNN classifier and train it using the noise-aware robust objective in Eq. (11). This objective down-weights supervision from suspicious target nodes while preserving reliable signals from clean nodes, thereby mitigating the impact of detection noise. The final output is a GNN classifier robust to both subgraph-based and feature-based graph backdoor attacks.

B.2 Time Complexity Analysis

We analyze the time complexity of CoGBD and compare the pre-training process of the consistency reconstruction model with DOMINANT [6], a representative reconstruction-based anomaly detector for the attributed networks. The analysis focuses on the computational cost of a single forward pass. Specifically, N and E denote the number of nodes and edges, respectively. F denotes the input feature dimension. d denotes the hidden dimension.

Consistency Reconstruction Model Pretraining. The model adopts an auto-encoder architecture with a two-layer GCN graph encoder and two lightweight MLP decoders with two layers. The encoding cost is $O(E \cdot d(F + d))$. Both decoders operate in a node-wise manner, resulting in a cost of $O(N \cdot d \cdot F)$, while the neighborhood branch additionally requires one mean pooling operation with cost $O(E \cdot d)$. The three reconstruction objectives further introduce $O(E \cdot F + N \cdot F)$ element-wise operations. As a result, the overall time complexity of the consistency reconstruction model per forward pass is $O(E \cdot d(F + d) + N \cdot d \cdot F)$, which scales linearly with the number of nodes and edges.

Comparison with DOMINANT. DOMINANT also follows an auto-encoder architecture. However, it explicitly reconstructs the adjacency matrix and optimizes $\|\hat{\mathbf{A}} - \mathbf{A}\|_F^2$, which incurs a dominant cost of $O(N^2 \cdot d)$. As a result, its overall time complexity per forward pass is $O(E \cdot d(F + d) + N^2 \cdot d)$, which scales quadratically with the number of nodes. In contrast, CoGBD avoids explicit adjacency reconstruction, making it more scalable for large graphs while retaining effective anomaly detection capability.

Detection. Given the pretrained reconstruction model, computing reconstruction errors in Eq. (7) involves only element-wise operations over node features and neighborhood representations, costing $O(N \cdot F)$. Selecting the top- $\rho\%$ backdoors can be implemented by sorting, costing $O(N \log N)$. Removing edges incident to suspicious trigger nodes requires scanning edges once, costing $O(E)$. Thus, the identification step costs $O(NF + N \log N + E)$.

Noise-aware Robust Training. An L -layer GNN classifier incurs per-forward cost $O(L \cdot E \cdot d^2 + L \cdot N \cdot d^2)$ in general. For the propagation in GCN, this is commonly dominated by sparse message passing $O(L \cdot E \cdot d^2)$. The noise-aware reweighting in Eq. (11) is node-wise and costs $O(N)$, which is negligible compared to message passing. Therefore, robust training has per-forward complexity $O(L \cdot E \cdot d^2)$.

Overall Complexity. Combining consistency reconstruction model pretraining, detection, and noise-aware robust training, the overall complexity of CoGBD is $O(E \cdot d(F + d) + N \cdot dF + NF + N \log N + E + L \cdot E \cdot d^2)$. In typical settings where $F = O(d)$, the overall cost is dominated by sparse message passing in the reconstruction encoder and the robust GNN classifier, i.e., $O(E \cdot d^2 + L \cdot E \cdot d^2)$, which scales linearly with E .

C Additional Experimental Setups

C.1 Attack Methods.

We consider three representative subgraph-based GBAs (GTA [29], UGBA [5], and DPGBA [35]) and one recent feature-based GBA (SPEAR [7]). A brief overview of each attack is provided below.

1. **GTA.** GTA is an early graph backdoor attack that introduces adaptive, sample-specific subgraph triggers via a trigger generator optimized to minimize the backdoor attack loss.
2. **UGBA.** UGBA improves attack efficiency by selecting representative target nodes through clustering. It further employs a similarity-constrained trigger generator that enforces feature similarity between trigger nodes and their attached target nodes, enhancing attack stealthiness.

3. **DPGBA.** DPGBA advances subgraph-based attacks by generating in-distribution triggers via adversarial learning, making trigger nodes harder to distinguish from clean ones.
4. **SPEAR.** SPEAR first identifies critical feature dimensions via a global importance-driven selection strategy, and then injects crafted feature-level triggers to maximize the attack success rate while preserving the original graph topology.

C.2 Defense Methods.

We select three representative defense methods that are specifically designed for graph backdoor attacks: Prune [5], Outlier Detection (OD) [35], and RIGBD [36].

1. **Prune.** Prune removes edges that connect low-similarity node pairs, based on the assumption that such edges are more likely to be introduced by a subgraph triggers.
2. **OD.** OD employs a commonly used outlier detector, DOMINANT [6], to identify out-of-distribution nodes and removes the edges associated with detected anomalies.
3. **RIGBD.** RIGBD first identifies poisoned target nodes by computing prediction variance over K inference runs. It then estimates the target label and suppresses the confidence of suspicious nodes toward the predicted target class to mitigate the backdoor effect.

Following [36], we also include a strong baseline that aims to learn a clean model directly from backdoor-poisoned data: ABL [18].

1. **ABL.** ABL is motivated by the observation that backdoor patterns are learned significantly faster than clean patterns during training, and that stronger attacks lead to faster convergence on poisoned data. Based on this, ABL proposes a two-stage anti-backdoor learning scheme that employs local gradient ascent (LGA) to first isolate backdoor samples at an early stage and then weaken the correlation between backdoor triggers and the target class, enabling the model to recover clean decision boundaries from poisoned data.

We further include three representative robust GNNs: Randomized Smoothing (RS) [25], GNNGuard [33], and RobustGCN [39].

1. **RS.** RS was originally proposed to defend against adversarial structural perturbations. The core idea is to construct a smoothed classifier by randomly dropping edges and aggregating predictions over multiple randomized graph instances. Following [36], we adopt this method as a baseline and set the edge drop ratio to be 0.5 to balance defense effectiveness and clean accuracy.
2. **GNNGuard.** GNNGuard adversarial structural perturbations by leveraging node similarity to reweight and prune edges. By dynamically adjusting edge importance during message passing, it suppresses the influence of adversarial connections and enables more robust propagation.
3. **RobustGCN.** RobustGCN improves the robustness of GCNs against adversarial attacks by modeling node representations as Gaussian distributions rather than deterministic vectors. Adversarial perturbations are absorbed into the variances of these distributions, thereby reducing their impact on the learned representations. In addition, RobustGCN introduces a variance-based attention mechanism that

assigns lower aggregation weights to uncertain neighborhoods, effectively suppressing the propagation of adversarial effects through message passing.

C.3 Implementation Details.

Computing Infrastructure. All methods are implemented using NumPy 1.26.3, PyTorch 2.7.1, and PyTorch Geometric 2.6.1. Experiments are conducted on a Linux server equipped with two Intel Xeon Silver 4314 CPUs and an NVIDIA RTX A5000 GPU with 24 GB of memory.

Attacks. For subgraph-based attacks, following [5, 35, 36], the trigger size is fixed to three nodes across all datasets. For the feature-based attack SPEAR, following [7], the trigger dimension is set to $\max(0.02F, 5)$, where F denotes the node feature dimension. A two-layer MLP is used as the trigger generator, and a two-layer GCN serves as the surrogate model. We tune their learning rates from $\{0.0001, 0.001, 0.01, 0.05\}$ and hidden dimensions from $\{16, 32, 64, 128\}$. All remaining hyperparameters follow the default settings of the official implementations.

Defense. For CoGBD, we adopt a two-layer GCN as the graph encoder, together with two separate two-layer MLPs as decoders for node attribute and neighborhood reconstruction. At the detection stage, the suspicious node ratio is set to $\rho = 3\%$ by default. During noise-aware robust training, a two-layer GCN is used as the backbone classifier. The reconstruction weights α and β are both selected from $\{2^{-4}, 2^{-3}, \dots, 2^4\}$. The temperature parameter τ is varied from 0.1 to 1.0 in increments of 0.1, and the unlearning weight λ is varied from 0.0 to 1.0 with the same step size. Each experiment is repeated five times with different random seeds, and we report the average results.

D Additional Experimental Results

D.1 Results on Clean Graph

In this section, we evaluate the clean-graph performance of CoGBD to verify that the proposed defense does not sacrifice predictive accuracy in the absence of backdoor attacks. To this end, we remove all backdoor triggers from the poisoned graph and train both a standard GCN and CoGBD on the resulting clean graph. The results are reported in Table 6. As shown in the table, CoGBD achieves clean accuracy that is comparable to, and in some cases slightly higher than, that of the vanilla GCN. This observation indicates that the proposed defense preserves effective supervision when no malicious perturbations are present. The underlying reason lies in the behavior of the noise-aware robust objective in Eq. (11). On clean graphs, reconstruction errors exhibit limited discriminability across nodes, which leads to nearly uniform noise-aware weights. Consequently, the objective performs only mild reweighting instead of aggressively down-weighting or removing nodes. This soft reweighting preserves the majority of informative training signals, thereby maintaining high clean accuracy.

D.2 Performance with Different Attack Budgets

In this section, we study the defense performance and detection ability under varying attack budgets, including the number of poisoned target nodes and the size of triggers.

Table 6: Comparison of clean accuracy between GCN and CoGBD trained on clean graphs.

Model	Cora	Pubmed	Flickr	OGB- <i>arxiv</i>
GCN	83.93	85.16	45.09	65.17
CoGBD	83.56	84.32	44.65	65.43

Table 7: Results for defense and backdoors detection with different $|\mathcal{V}_B|$.

Attacks	$ \mathcal{V}_B $	ASR	ACC	Recall _{tar}	Recall _{tri}
GTA	113	95.44 06.10	65.63	89.20	100.00
	339	97.97 00.00	65.20	100.00	100.00
	565	99.96 00.01	65.20	100.00	100.00
	791	99.97 00.27	65.02	100.00	100.00
	1,017	99.93 00.27	64.92	97.92	100.00
UGBA	113	93.42 03.55	65.26	80.01	100.00
	339	95.49 03.09	65.29	78.88	100.00
	565	97.55 00.98	65.37	65.55	100.00
	791	98.26 00.66	65.49	66.89	100.00
	1,017	98.24 05.41	64.35	59.00	100.00
DPGBA	113	93.69 00.00	65.05	84.07	100.00
	339	95.53 00.00	65.90	84.42	100.00
	565	96.32 00.00	65.89	77.01	69.56
	791	97.27 00.00	65.88	71.08	72.06
	1,017	97.29 00.00	65.00	73.19	67.65
SPEAR	113	96.29 00.06	66.83	99.07	-
	339	96.72 00.03	66.73	99.70	-
	565	96.78 00.00	66.66	94.73	-
	791	97.37 00.91	66.75	85.15	-
	1,017	97.86 03.90	66.78	76.59	-

Varying the Number of Target Nodes. We first examine how increasing the number of poisoned target nodes affects the performance of CoGBD. In particular, we set the number of \mathcal{V}_B to $\{113, 339, 565, 791, 1017\}$ for OGB-*arxiv* under four representative GBAs. We report the ASR before and after defense, together with ACC and the recall of target and trigger nodes. The results are shown in Table 7. From the table, we observe: (1) CoGBD consistently achieves high recall for both target nodes and trigger nodes across different numbers of target nodes. In most cases, the model prioritizes the identification of trigger nodes, which can be attributed to the fact that trigger nodes in subgraph-based attacks typically exhibit more pronounced feature-based homophily discontinuities than target nodes, making them easier to detect. (2) CoGBD maintains low attack success rates and comparable clean accuracy throughout all settings. Even when the number of target nodes increases to 1024, where a slight decline in target-node recall can be observed, the overall defense performance remains robust. This stability stems from the proposed noise-aware training strategy, which mitigates the impact of detection noise and prevents performance degradation under increasing attack strength.

Varying the Size of Triggers. We now conduct experiments to investigate how different trigger sizes impact the performance of CoGBD. Specifically, we set the trigger size to $\{1, 2, 3, 4, 5\}$ and conducted experiments on the OGB-*arxiv* dataset. We report the ASR before and after defense, together with ACC and the recall of

Table 8: Results for defense and backdoors detection with different trigger size.

Attacks	Trigger Size	ASR	ACC	Recall _{tar}	Recall _{tri}
GTA	1	93.19 00.12	63.95	35.83	100.00
	2	99.89 00.00	64.02	100.00	100.00
	3	100.0 00.00	64.44	100.00	100.00
	4	100.0 00.01	64.44	100.00	100.00
	5	99.98 00.00	64.08	99.82	100.00
UGBA	1	83.54 01.80	64.29	51.95	100.00
	2	97.09 00.21	64.48	80.08	100.00
	3	97.77 02.03	64.33	90.12	100.00
	4	97.84 00.82	64.51	90.18	100.00
	5	97.73 05.20	64.26	90.12	100.00
DPGBA	1	92.47 00.00	64.89	61.95	100.00
	2	95.10 00.00	64.91	65.96	93.98
	3	96.16 00.01	65.02	77.01	69.56
	4	97.10 00.00	65.08	88.59	19.65
	5	97.65 00.01	65.02	93.76	18.23
SPEAR	1	96.17 00.01	66.72	89.92	-
	2	96.29 00.03	66.73	95.64	-
	3	96.61 00.00	66.68	95.27	-
	4	97.09 00.00	66.79	97.82	-
	5	97.88 00.01	66.72	97.45	-

target and trigger nodes. The results are in Tab 8. From the table, we observe that CoGBD consistently achieves low ASR and high clean accuracy across all trigger sizes, demonstrating effective defense without sacrificing benign performance. As the trigger size increases, the attack success rate tends to rise; however, larger triggers are also less stealthy. This reduced stealthiness is reflected by the increasing recall of both trigger nodes and target nodes, as larger trigger subgraphs induce more pronounced structural-semantic inconsistencies that are easier to detect. When the trigger size is small (e.g., trigger size = 1), the attack becomes more stealthy. In this case, subgraph-based GBAs introduce weaker semantic discontinuities on target nodes, making them harder to identify, as evidenced by the lower Recall_{tar} on GTA and UGBA (e.g., 35.83% and 51.95%, respectively). Despite this, CoGBD still maintains strong defense performance, which can be attributed to the proposed noise-aware mechanism that effectively mitigates the impact of detection error.

D.3 More Results of the Ability to Detect Backdoors

In this section, we provide additional results of the ability to detect backdoors on the Cora, PubMed, and Flickr datasets. We present the Recall_{tar} and Recall_{tri}, together with Clean ACC (which is trained on the clean graph), ASR, and ACC as reference metrics. The results are shown in Table 9. From the table, we make two main observations: (1) CoGBD consistently achieves high recall on target nodes across different datasets and attack types. This strong target-node detection capability plays a dominant role in effectively suppressing ASR, as identifying and mitigates the influence of target nodes, directly disrupt the backdoor attack objective. (2) In some cases, the recall of trigger nodes is relatively lower, such as 33.33% on Pubmed under UGBA. This behavior can be attributed to the increased stealthiness of triggers on certain datasets, where trigger

Table 9: Results for the ability to detect Backdoors.

Attacks	Dataset	Clean ACC	ASR	ACC	Recall _{tar}	Recall _{tri}
GTA	Cora	83.93	0.0	83.48	100.00	33.33
	Pubmed	85.16	0.89	85.20	76.00	100.00
	Flickr	45.09	0.0	45.36	96.75	33.33
UGBA	Cora	83.93	0.0	84.30	80.0	70.83
	Pubmed	85.16	1.12	84.33	88.81	33.33
	Flickr	45.09	0.0	44.36	100.00	33.33
DPGBA	Cora	83.93	0.0	84.67	74.24	64.17
	Pubmed	85.16	0.0	85.47	78.20	100.00
	Flickr	45.09	0.0	43.19	85.62	100.00
SPEAR	Cora	83.93	0.0	83.41	100.00	-
	Pubmed	85.16	7.27	84.76	100.00	-
	Flickr	45.09	0.0	43.62	100.00	-

nodes exhibit weaker structural-semantic irregularities and are therefore harder to distinguish from clean nodes. Nevertheless, the overall defense performance of CoGBD is not compromised, as the proposed noise-aware training mechanism can still effectively mitigate backdoor effects under imperfect detection.

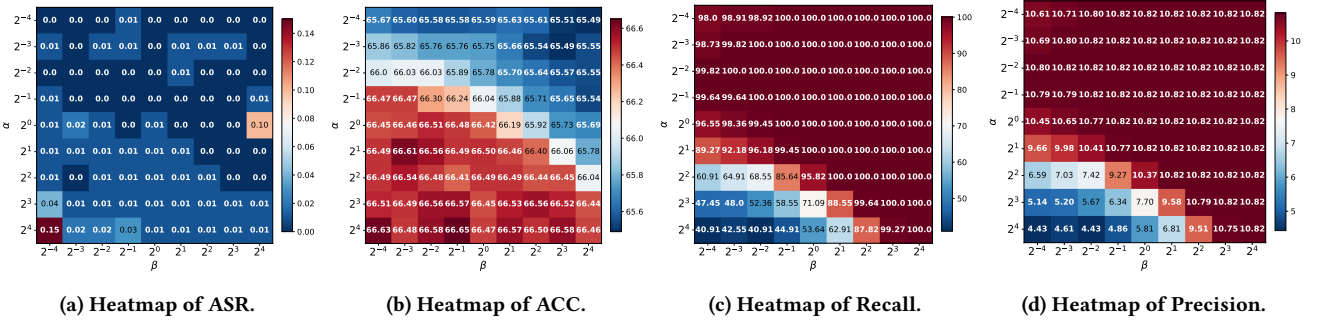
D.4 More Experiments of Parameter Sensitivity

Parameter Sensitivity of α and β under Feature-based GBAs.

Following the same setup as in Sec. 6.5, we vary the reconstruction weights α and β from 2^{-4} to 2^4 and evaluate CoGBD under the feature-based SPEAR attack on OGB-arxiv. Fig. 5 reports ASR, ACC, Recall_{tar}, and Precision. Across a wide range of α and β , CoGBD consistently maintains near-zero ASR. This demonstrates the strong robustness of our CoGBD under feature-based GBAs. This behavior stems from the nature of SPEAR, which injects triggers directly into node attributes while preserving graph structure, thereby introducing pronounced structure-feature inconsistencies around poisoned nodes. All three reconstruction signals in CoGBD are inherently sensitive to such inconsistencies, enabling effective detection of poisoned nodes and reliable suppression of backdoor activation. We also observe that detection precision can be relatively low due to the small fraction of poisoned nodes. Nevertheless, CoGBD preserves high clean accuracy across all settings, indicating that the noise-aware robust training stage is tolerant to noisy detection results and prevents excessive penalization of clean nodes.

Parameter Sensitivity Analysis of ρ .

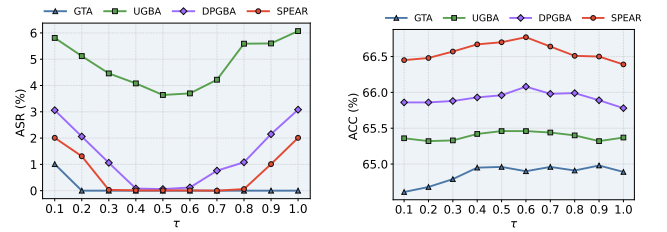
We analyze the effect of ρ , which controls the proportion of nodes treated as suspicious during detection. Specifically, we vary ρ over {10%, 8%, 5%, 3%, 1%} and report ASR, ACC, Recall_{tar}, and Recall_{tri} on OGB-arxiv in Table 10. Our results show that, as ρ decreases, the recall on both poisoned target nodes and trigger nodes naturally declines, since fewer nodes are inspected as potential anomalies. Notably, this reduction in recall does not necessarily impair the ability of CoGBD to suppress ASR, indicating that effective backdoor mitigation does not require exhaustive detection of all backdoors. When ρ is too large (e.g., 10%), excessive false positives are introduced, which injects training noise and can degrade robustness (e.g., a ASR of 24.37% under GTA). Conversely, an overly small ρ (e.g., 1%) leads to more false

Figure 5: Sensitivity analysis of weights: α and β .Table 10: Results for defense and backdoors detection with different ρ .

Attack	$\rho\%$	ASR	ACC	Recall _{tar}	Recall _{tri}
GTA	1%	0.00	65.08	2.85	100.00
	3%	0.00	65.11	100.00	100.00
	5%	0.00	65.18	100.00	100.00
	8%	0.00	64.26	100.00	100.00
	10%	24.37	63.55	100.00	100.00
UGBA	1%	0.00	65.28	0.00	100.00
	3%	0.09	65.38	91.27	100.00
	5%	0.87	64.27	91.88	100.00
	8%	0.18	64.19	96.42	100.00
	10%	0.30	64.13	97.77	100.00
DPGBA	1%	0.00	65.82	52.58	18.05
	3%	0.00	65.97	80.01	69.56
	5%	0.01	64.00	85.03	88.50
	8%	0.01	64.13	88.95	97.35
	10%	0.01	64.16	90.02	98.58
SPEAR	1%	0.00	66.60	100.00	–
	3%	0.00	66.35	100.00	–
	5%	0.00	66.42	100.00	–
	8%	0.00	66.49	100.00	–
	10%	0.00	66.31	100.00	–

negatives, resulting in missed poisoned targets (e.g., Recall_{tar} = 0 under UGBA). Overall, these results suggest that CoGBD is robust to partial detection and can effectively eliminate backdoor effects without identifying all anomalous patterns. In our experiments, $\rho = 3\%$ provides a favorable trade-off between detection coverage and robustness across most GBA settings.

Parameter Sensitivity Analysis of τ . We study the effect of τ , which controls the sharpness of the noise-aware node weights. Specifically, we vary τ from 0.1 to 1.0 with a step size of 0.1 and evaluate CoGBD on OGB-arxiv under four representative GBAs, reporting ASR and ACC in Fig. 6. As τ increases, ASR first decreases and then increases, while ACC exhibits the opposite trend, indicating a clear trade-off between backdoor suppression and clean performance. When τ is too small, node confidence scores become insufficiently discriminative, leading to weaker suppression of poisoned nodes and higher ASR (e.g., 5.81% ASR on UGBA at $\tau = 0.1$). In contrast, overly large τ enforces excessively sharp penalties on



(a) The results of ASR(%).

(b) The results of ACC(%).

Figure 6: Sensitivity analysis of τ .

suspicious nodes, amplifying the impact of false positives and introducing training noise, which again degrades robustness (e.g., 6.07% ASR on UGBA at $\tau = 1.0$). Overall, moderate values of τ provide the best balance between robustness and accuracy. In our experiments, $\tau \in [0.4, 0.6]$ consistently achieves low ASR while preserving high clean accuracy across different attack settings.

D.5 Impact of GNN backbones.

To evaluate the flexibility of CoGBD across different GNN architectures, we replace the default GCN backbone in the noise-aware robust training stage with alternative backbones, including GAT [24] and GraphSAGE [10]. The results are reported in Table 11. Across all backbones and datasets, CoGBD consistently achieves low attack success rates while maintaining clean accuracy that is comparable to, and in some cases slightly higher than, the corresponding vanilla GNNs. These results indicate that the CoGBD does not rely on architecture-specific properties and can be seamlessly integrated with diverse GNN backbones. Overall, CoGBD exhibits strong flexibility and transferability as a general backdoor defense framework.

E Additional Related Works

Graph Backdoor Attacks. Recent studies [5, 7, 29, 34, 35] have demonstrated that graph neural networks (GNNs) are vulnerable to backdoor attacks, posing serious security risks in high-stakes domains where incorrect predictions may lead to severe consequences. In a graph backdoor attack (GBA), an adversary implants trigger patterns into a small subset of training nodes such that the trained model associates the trigger with a predefined target label. At test time, nodes carrying the trigger are misclassified into the target

Table 11: Results of different GNN backbones with CoGBD.

Attacks	Defense	Cora		Pubmed		Flickr		OGB-arxiv	
		ASR(%)↓	ACC(%)↑	ASR(%)↓	ACC(%)↑	ASR(%)↓	ACC(%)↑	ASR(%)↓	ACC(%)↑
GTA	GAT	82.66	82.46	90.77	82.60	100.00	40.05	90.69	63.22
	GraphSAGE	96.96	81.22	99.98	84.57	100.00	46.04	96.62	67.05
	CoGBD _{GAT}	7.49	83.56	1.22	82.87	0.00	40.35	0.19	63.66
	CoGBD _{GraphSAGE}	2.29	82.89	4.10	85.57	0.00	45.87	0.00	67.34
UGBA	GAT	100.00	84.89	98.67	83.05	100.00	40.22	90.68	63.03
	GraphSAGE	97.78	81.12	99.08	84.05	100.00	45.15	98.66	64.88
	CoGBD _{GAT}	3.91	84.15	5.13	82.84	0.00	40.35	0.00	64.60
	CoGBD _{GraphSAGE}	3.70	82.81	5.97	83.36	0.00	46.06	1.47	66.95
DPGBA	GAT	91.08	83.33	95.54	83.56	100.00	40.35	91.98	63.02
	GraphSAGE	90.48	83.35	93.08	84.01	100.00	44.35	90.04	64.56
	CoGBD _{GAT}	2.41	83.78	5.45	81.60	0.00	40.35	0.04	64.11
	CoGBD _{GraphSAGE}	4.80	82.15	1.76	85.40	0.00	43.64	0.00	68.02
SPEAR	GAT	98.82	82.45	95.03	85.06	100.00	40.33	96.95	64.56
	GraphSAGE	96.72	84.08	92.43	85.42	100.00	44.46	97.88	65.55
	CoGBD _{GAT}	0.00	82.44	7.40	83.03	0.00	40.35	0.37	64.39
	CoGBD _{GraphSAGE}	3.47	84.33	3.83	85.12	0.00	46.21	0.02	67.37

class, while predictions on clean nodes remain largely unaffected. In backdoor attacks, triggers are typically constructed from the basic elements of data samples. Analogous to pixel-level visual patterns in computer vision [3, 9, 17] and token-level triggers in natural language processing [20, 21], subgraphs naturally serve as triggers in graph data [4, 29, 34, 37]. Accordingly, most existing GBAs instantiate triggers as subgraphs by manipulating local connectivity patterns. SBA [34] injects a fixed or sampled subgraph triggers, whereas GTA [29] learns adaptive, sample-specific triggers via a generator. UGBA [5] further enhances attack stealthiness by explicitly enforcing feature similarity between trigger nodes and the attached poisoned target nodes. Subsequent studies reveal that many such subgraph-based triggers remain out-of-distribution and are thus detectable [35], motivating DPGBA [35] to generate in-distribution triggers through adversarial optimization. Beyond structural manipulation, feature-based GBAs inject triggers directly into node attributes while preserving the original graph topology. SPEAR [7] exemplifies this direction and poses greater challenges to existing defenses, as it introduces no explicit structural anomalies and relies purely on feature-level perturbations. From a supervision perspective, the aforementioned methods primarily operate under the dirty-label setting, where poisoned nodes are explicitly relabeled to the target class during training. This setting simplifies attack construction but is less stealthy due to explicit label manipulation. More recently, several works [30, 31] have explored the clean-label setting, in which training labels remain unchanged. Instead, attackers rely on subtle trigger-induced representation shifts to cause misclassification at test time. Moreover, recent studies [16, 26] extend GBAs to the multi-target setting, where multiple target labels are attacked simultaneously. Compared with single-target attacks, multi-target GBAs require learning more complex and potentially overlapping trigger-label associations, which increases both the attack surface and the difficulty of defense. This

setting further exacerbates the challenge for existing defenses, as abnormal patterns may be distributed across different target classes rather than concentrated around a single label.